Assessing the formation and evolution mechanisms of severe haze pollution in Beijing-Tianjin-Hebei region by using process analysis

Lei Chen[1,2], Jia Zhu[1], Hong Liao[1], Yi Gao[3], Yulu Qiu[4,5], Meigen Zhang[3,6,7], Zirui Liu[3], Nan Li[1], and Yuesi Wang[3,7]

[1]Jiangsu Key Laboratory of Atmospheric Environment Monitoring and Pollution Control, Jiangsu Collaborative Innovation Center of Atmospheric Environment and Equipment Technology, School of Environmental Science and Engineering, Nanjing University of Information Science & Technology, Nanjing, 210044, China

[2]Key Laboratory of Meteorological Disaster, Ministry of Education (KLME), Joint International Research Laboratory of Climate and Environment Change (ILCEC), Collaborative Innovation Center on Forecast and Evaluation of Meteorological Disasters (CIC-FEMD), Nanjing University of Information Science & Technology, Nanjing, 210044, China

[3]State Key Laboratory of Atmospheric Boundary Layer Physics and Atmospheric Chemistry, Institute of Atmospheric Physics, Chinese Academy of Sciences, Beijing, 100029, China

[4]Institute of Urban Meteorology, China Meteorological Administration, Beijing 100089, China

[5]Beijing Shangdianzi Regional Atmosphere Watch Station, Beijing, China

[6]University of Chinese Academy of Sciences, Beijing, 100049, China

[7]Center for Excellence in Regional Atmospheric Environment, Institute of Urban Environment, Chinese Academy of Sciences, Xiamen, 361021, China

Correspondence to: H. Liao (hongliao@nuist.edu.cn)

Abstract. Fine-particle pollution associated with haze threatens human health, especially in the North China Plain, where extremely high $PM_{2.5}$ concentrations were frequently observed during winter. In this study, the WRF-Chem model coupled with an improved integrated process analysis scheme was used to investigate the formation and evolution mechanisms of a haze event over Beijing-Tianjin-Hebei (BTH) in December 2015, including examining the contributions of local emission and regional transport to the $PM_{2.5}$ concentration in BTH, and the contributions of each detailed physical or chemical process to the variations in the $PM_{2.5}$ concentration. The influence mechanisms of aerosol radiative forcing (including aerosol direct and indirect effects) were also examined by using the process analysis. During the aerosol accumulation stage (December 16-22, Stage_1), the near-surface $PM_{2.5}$ concentration in BTH was increased from 24.2 μg m^{-3} to 289.8 μg m^{-3}, with the contributions of regional transport increased from 12% to 40%, while the contributions of local emission were decreased

from 59% to 38%. During the aerosol dispersion stage (December 23-27, Stage_2), the average concentration of $PM_{2.5}$ was 107.9 µg m^{-3}, which was contributed by local emission of 51% and regional transport of 24%. The 24-h change (23:00LST minus 00:00LST) in the near-surface $PM_{2.5}$ concentration was +43.9 µg m^{-3} during Stage_1 and -41.5 µg m^{-3} during Stage_2. Contributions of aerosol chemistry, advection and vertical mixing to the 24-h change were +29.6 (+17.9) µg m^{-3}, -71.8 (-103.6) µg m^{-3} and -177.3 (-221.6) µg m^{-3} during Stage_1 (Stage_2), respectively. Small differences in contributions of other processes were found between Stage_1 and Stage_2. Therefore, the $PM_{2.5}$ increase over BTH during haze formation stage was mainly attributed to the strong production by aerosol chemistry process and weak removal by advection and vertical mixing processes. When aerosol radiative feedback was considered, the 24-h $PM_{2.5}$ increase was enhanced by 4.8 µg m^{-3} during Stage_1, which could be mainly attributed to the contributions of vertical mixing process (+22.5 µg m^{-3}), advection process (-19.6 µg m^{-3}) and aerosol chemistry process (+1.2 µg m^{-3}). The restrained vertical mixing was the primary reason for the enhancement in near-surface $PM_{2.5}$ increase when aerosol radiative forcing was considered.

1 Introduction

Anthropogenic activities associated with rapidly developed industrialization and urbanization have been leading to a sustained increase in the amounts of atmospheric pollutants, especially in the fast-developing countries (IPCC, 2013). As one of the largest emission sources of aerosols and their precursors, China has been suffering from serious air pollution for years (Lei et al., 2011; Li et al., 2011; Liu et al., 2018a), with severe haze events frequently occurring in winter, especially over large urban agglomerations, such as the North China Plain (NCP) (Han et al., 2014; Gao et al., 2015), the Yangtze River Delta area (YRD) (Ding et al., 2016; Wang et al., 2016a), and the Sichuan Basin (SCB) (Zhao et al., 2018; Zhang et al., 2019). During severe haze events, the observed maximum hourly surface-layer $PM_{2.5}$ (fine particulate matter with aerodynamic diameter of 2.5 μm or less) concentration exceeded 1000 μg m^{-3} (Wang et al., 2013b; Sun et al., 2016; Li et al., 2017a), which could significantly influence visibility (Li et al., 2014), radiation budget (Steiner et al., 2013), atmospheric circulation (Jiang et al., 2017), cloud properties (Unger et al., 2009), and human health (Hu et al., 2014; Guo et al., 2017).

Extensive studies have been carried out in recent years to analyze the formation mechanisms of haze episodes in China. Wang et al. (2013a) used a synergy of ground-based observations, satellite, and lidar measurements to study a long-lasting and severe haze episode occurred in eastern China in January 2013, and concluded that stagnant meteorological conditions, which could be generally characterized by weak wind speed, high relative humidity, intense inversion, and low mixing layer height, were tightly associated with severe haze episodes. Based on National Center for Environmental Prediction (NCEP) reanalysis data, Shu et al. (2017) identified five typical synoptic patterns, and pointed out that each synoptic pattern exerted different impacts on particle pollution over YRD. By analyzing the simulation results from a large ensemble climate model (MIROC5), Li et al. (2018a) investigated the contributions of anthropogenic influence to severe haze events happened over eastern China in January 2013 and December 2015, and found that anthropogenic forcing (i.e., increased emissions of greenhouse gases) could modify atmospheric circulation pattern, and these human-induced circulation changes were conducive to the occurrence of severe haze events. Zhang et al. (2015a) used a global 3-D chemical transport model (GEOS-Chem) to quantify the local source contributions to wintertime surface-layer $PM_{2.5}$ concentrations over North China from 2013 to 2015, and reported that emissions from residential and industrial sources and transportation contributed most to the high concentrations of atmospheric aerosols in Beijing. Many studies reported that regional transport of aerosols also

played an important role in haze episodes (Wang et al., 2013b; Jiang et al., 2015; Li et al., 2018b). Wang et al. (2013b) reported that the cross-city clusters transport outside BTH (Beijing, Tianjin, and Hebei) and transport among cities inside BTH contributed 20%-35% and 26%-35% of $PM_{2.5}$ concentrations over BTH, respectively. Secondary aerosol formation and their hygroscopic growth were also confirmed to be a large contributor to severe haze episodes (Huang et al., 2014b; Han et al., 2015; Chen et al., 2019a). The conversion of SO_2 to SO_4^{2-} was strongly associated with high relative humidity, and NO_3^- was found to be produced mainly by photochemical and heterogeneous reactions (Chen et al., 2016; Zhang et al., 2018a).

It is well known that aerosols can scatter and absorb solar radiation to alter the radiative balance of the atmosphere and surface (direct radiative effect), and can serve as cloud condensation nuclei or ice nuclei to affect cloud properties (indirect radiative effect) (Twomey, 1974). These impacts are coupled with atmospheric dynamics to produce a chain of interactions with a large range of meteorological variables that influence both weather and climate (Ramanathan et al., 2001; Huang et al., 2006; Li et al., 2017c; Yang et al., 2017), which will further induce feedbacks on aerosol production, accumulation, and even severe haze pollutions (Petaja et al., 2016; Li et al., 2017d; Zhao et al., 2017; Gao et al., 2018; Lou et al., 2019). Based on multi-year measurements (from 2010 to 2016), Huang et al. (2018) found that aerosol radiative effects led to a significant heating in the upper planetary boundary layer (PBL) and a substantial dimming at the surface over North China. This is because high concentrations of light-absorbing aerosols were observed, and the aerosol-meteorology interactions depressed the development of PBL, and therefore aggravated the haze pollution (Su et al., 2018). The light-absorbing aerosols can also amplify haze in NCP by weakening East Asian winter monsoon wind speeds through ocean and cloud feedbacks (Lou et al., 2019). By using the WRF-Chem model, Gao et al. (2015) analyzed the feedbacks between aerosols and meteorological fields over NCP in January 2013, and found that aerosols caused a significant negative (positive) radiative forcing at the surface (in the atmosphere), resulting in a weaker surface-layer wind speed and lower PBL height (PBLH). The average surface-layer $PM_{2.5}$ concentration was increased by 10-50 μg m^{-3} as a result of the more stable atmosphere. By analyzing the observations from a comprehensive field experiment and simulation results from WRF-Chem model, Liu et al. (2018b) concluded that the decreased PBLH associated with increased aerosol concentrations could enhance surface-layer relative humidity by weakening the vertical transport of water vapor, and the increased relative humidity at the surface accelerated the formation

4

of secondary particulate matters through heterogeneous reactions, leading to the increase of the PM$_{2.5}$ concentration by 63 μg m^{-3} averaged over the NCP during 15-21 December, 2016.

All these studies discussed above revealed that the formation of haze episode was caused by the synergy impacts of local emissions, regional transport, meteorological conditions, and chemical production. Nevertheless, only the net combined effects on the concentrations of pollutants were provided, without the capabilities of understanding and isolating the atmospheric physical and chemical processes involved. The quantitative assessment of the contributions from each detailed physical/chemical process (e.g., vertical mixing process, advection process, emission source process, aerosol chemistry process, cloud chemistry process) is necessary for fully understanding of the formation and evolution mechanisms of haze episodes (Goncalves et al., 2009; Xing et al., 2017; Kang et al., 2019). What's more, although many previous studies have identified the positive feedback effects of aerosol radiative forcing on particulate accumulation, the detailed influence mechanisms of the forcing-response relationship at each process chain remain largely elusive (i.e., the prominent physical or chemical processes responsible for the aerosol radiative impacts on haze episodes). Since 2013, substantial efforts have been taken to improve air quality in China, including emission reduction and energy transition. However, haze events continued to occur frequently all over the country. For example, a severe, long-lasting, and wide-ranging haze episode was observed in December 2015 over the central and eastern China, with the regional average PM$_{2.5}$ concentration exceeding 150 μg m^{-3}. For BTH, a red alert for haze (the most serious level) was issued for the period from 20 to 22 December 2015, with the maximum hourly PM$_{2.5}$ concentration exceeding 1000 μg m^{-3}. The formation and evolution mechanisms, and the aerosol radiative feedbacks of this severe haze episode have not been fully estimated yet.

In this study, we develop an improved online integrated process rate (IPR) analysis scheme (i.e., process analysis) in the fully coupled online Weather Research and Forecasting-Chemistry (WRF-Chem) model, to investigate the formation and evolution mechanisms of the severe haze episode happened over NCP from 16 to 29 December 2015. Sensitivity experiments are conducted to examine the contributions of local emission and regional transport to the PM$_{2.5}$ concentrations during the haze episode, while the IPR analysis is used to quantify the contributions of each detailed physical/chemical process to the variations in the PM$_{2.5}$ concentrations. The effects of aerosol radiative forcing, including direct and indirect effects, on meteorological parameters and PM$_{2.5}$ levels during the haze episode are also quantified, with a special focus on

the detailed influence mechanism. We hope that the results concluded in this study may provide better understanding of the formation mechanisms for severe haze events, and help policy makers take targeted measures to improve air quality over North China.

This manuscript is arranged as follows. Model configuration, integrated process rate (IPR) analysis (i.e., process analysis), numerical experiments, and observations are presented in Section 2. Model evaluation is conducted in Section 3. The formation and evolution mechanisms of the haze episode are investigated in Section 4. Section 5 provides the impacts of aerosol radiative forcing. Summaries and discussions are presented in Section 6.

2 Methods

2.1 Model configuration

A fully coupled online Weather Research and Forecasting-Chemistry model (WRF-Chem v3.7) is used to simulate meteorological fields and concentrations of gases and aerosols simultaneously (Skamarock et al., 2008; Grell et al., 2005). The WRF-Chem model is designed with two domains using 219 (west-east) $\times$ 159 (south-north) and 150 (west-east) $\times$ 111 (south-north) grid points at the horizontal resolutions of 27 and 9 km, respectively (Fig. 1). The outer domain covers nearly the whole East Asia, and the inner domain is located in the NCP. In order to minimize the impacts from IBCs (lateral boundary conditions), we only analyze the simulation results from the inner region of the second domain (i.e., BTH), following Chen et al. (2018) and Wu et al. (2012). The vertical dimension is resolved by 29 full sigma levels, with 15 layers located in the lowest 2 km for finer resolution in the planetary boundary layer, and the height of the first layer averaged in BTH is about 30 m.

Meteorological initial and lateral boundary conditions used in the WRF-Chem model are taken from the NCEP (National Center for Environmental Prediction) Final Operational Global Analysis data with the spatial resolution of $1\degree \times 1\degree$. Four-dimensional data assimilation (FDDA) with the nudging coefficient of 3.0×10^{-4} for wind (in and above PBL), temperature (above PBL) and water vapor mixing ratio (above PBL) is adopted to improve the accuracy of simulation results (no analysis nudging is included for the inner domain) (Lo et al., 2008; Otte, 2008; Wang et al., 2016b; Werner et al., 2016).

The forecasts from the global chemical transport model MOZART-4 are processed to provide the chemical initial and boundary conditions for the WRF-Chem model (Emmons et al., 2010).

Anthropogenic emission data are obtained from the MIX Asian emission inventory (http://www.meicmodel.org/dataset-mix.html), with a horizontal resolution of 0.25 degree (Li et al., 2017b). It is developed to support the MICS-Asia III (Model Inter-Comparison Study for Asia Phase III) and the TF HTAP (Task Force on Hemispheric Transport of Air Pollution) projects. This inventory includes SO_2 (sulfur dioxide), NO_x (nitrogen oxides), CO (carbon monoxide), CO_2 (carbon dioxide), NMVOC (non-methane volatile organic compounds), NH_3 (ammonia), BC (black carbon), OC (organic carbon), $PM_{2.5}$ and PM_{10}. All these species are from several sectors, such as agriculture, industry, power, transportation and residential, and the emission rate of each species for each hour is based on Gao et al. (2015). The biogenic emissions are calculated online using the MEGANv2.04 (Model of Emission of Gases and Aerosol from Nature v2.04) model (Guenther, 2006). Biomass-burning emissions are obtained from the GFEDv3 (Global Fire Emissions Database v3) (Randerson et al., 2005). Dust emissions and sea salt emissions are calculated online by using algorithms proposed by Shao (2004) and Gong et al. (1997), respectively.

The Carbon-Bond Mechanism version Z (CBMZ) (Zaveri and Peters, 1999) is selected to simulate the gas phase chemistry, and the 8-bin sectional aerosol module, MOSAIC (Model for Simulating Aerosol Interactions and Chemistry) (Zaveri et al., 2008), with some aqueous chemistry, is used to simulate aerosol evolution. All major aerosol species are considered in the MOSAIC scheme, including sulfate (SO_4^{2-}), nitrate (NO_3^-), ammonium (NH_4^+), chloride (Cl), sodium (Na), BC, primary organic mass, liquid water, and other inorganic mass (Zaveri et al., 2008). The aerosol size distribution is divided into discrete size bins defined by their lower and upper dry particle diameters (Zhao et al., 2010). In the current CBMZ/MOSAIC scheme, the formation of SOA (secondary organic aerosol) is not included (Zhang et al., 2012; Gao et al., 2016). Aerosol optical properties, including extinction efficiency, single scatter albedo, and asymmetry factor are computed by Mie theory, based on aerosol composition, mixing state, and size distribution (Barnard et al., 2010). The impacts of aerosols on photolysis rates are calculated using the Fast-J photolysis scheme (Wild et al., 2010). Aerosol radiation is simulated by RRTMG (Rapid Radiative Transfer Model for GCMs) for both shortwave (SW) and longwave (LW) radiation (Zhao et al., 2011). More information about the parameterizations used in this study can be found in Table 1.

2.2 Integrated process rate (IPR) analysis

Most air quality models are configured to output only the pollutant concentrations that reflect the combined effects of all physical and chemical processes. Quantitative information of the impacts of individual process is usually unavailable. Process analysis techniques (i.e., integrated process rate (IPR) analysis) can be used in grid-based Eulerian models (e.g., WRF-Chem) to obtain contributions of each physical/chemical process to variations in pollutant concentrations. Eulerian models utilize the numerical technique of operator splitting to solve continuity equations for each species into several simple ordinary differential equations or partial differential equations that only contain the influence of one or two processes (Gipson, 1999).

The IPR analysis method has been fully implemented in Community Multi-scale Air Quality (CMAQ) model, and has been widely applied to study regional photochemical ozone (O_3) pollution (Goncalves et al., 2009; Khiem et al., 2010; Xing et al., 2017; Tang et al., 2017). Several WRF-Chem model studies used the IPR analysis to investigate the impacts of physical/chemical process on variations in O_3 concentrations. Gao et al. (2018) investigated the impacts of BC-PBL interactions on O_3 concentrations by analyzing the contributions from photochemistry, vertical mixing, and advection processes. Jiang et al. (2012) calculated the contributions of photochemical reactions and physical processes to O_3 formation by using a simplified IPR analysis scheme.

Applying the IPR analysis to diagnose the contributions of each physical or chemical process to variations in aerosol concentrations in WRF-Chem model is more complex technically, and therefore few studies conducted the IPR analysis for aerosols. In this study, we developed an improved IPR analysis scheme in the WRF-Chem model to isolate the processes impacting variations in aerosol concentrations into nine different processes, namely advection (TRAN), emission source (EMIS), dry deposition (DYRD), turbulent diffusion (DIFF), sub-grid convection (SGCV), gas-phase chemistry (GASC), cloud chemistry (CLDC), aerosol chemistry (AERC), and wet scavenging (WETP). TRAN includes horizontal and vertical advection, which is highly related to wind and aerosol concentration gradients from upwind regions to downwind areas (Gao et al., 2018). DRYD is based on resistance models for trace gases (Wesely, 1989) and aerosol particles (Ackermann et al., 1998). SGCV refers to the scavenging within the sub-grid wet convective updrafts. CLDC refers to aqueous-phase photolytic and radical chemistry reactions in clouds, including the activation processes. AERC means microphysical nucleation,

condensation, and coagulation, as well as the mass transfer between the gas phase and condensed phase. WETP contains in-cloud rainout and below-cloud washout during grid-scale precipitation. The contribution of individual process can be calculated as the difference of aerosol concentrations before and after the corresponding operator.

Based on the principle of mass balance, IPR can be verified by comparing the variations in aerosol concentrations (the concentration at the current time minus the concentration at the previous time) with the sum of the contributions from the nine processes during each time step. As shown in Fig. S1, the net contributions of all processes match the variations in aerosol concentrations pretty well.

2.3 Numerical experiments

Table 2 summarizes the experimental designs. To investigate the contributions of regional transport and local emission to the $PM_{2.5}$ concentrations in BTH, four simulations with different anthropogenic emission categories are conducted: (1) CTL: The control simulation with all anthropogenic emissions considered; (2) NoAnth: No anthropogenic emission is considered in the whole domain; (3) NoBTH_Anth: Same as CTL, but anthropogenic emissions in BTH are excluded; (4) OnlyBTH_Anth: Contrary to the NoBTH_Anth case, anthropogenic emissions are only considered in BTH. All the physical and chemical schemes used in these cases are identical. The contributions of regional transport and local emission to the $PM_{2.5}$ concentration in BTH can be identified by comparing the simulation results of NoBTH_Anth and NoAnth (i.e., NoBTH_Anth minus NoAnth) and OnlyBTH_Anth and NoAnth (i.e., OnlyBTH_Anth minus NoAnth), respectively.

To quantify the aerosol radiative effects (ARE) on haze pollution, another sensitivity experiment (referred to as NoARE case) is designed by turning off the feedbacks between aerosols and meteorological variables, including eliminating the aerosol direct effect (ADE) and aerosol indirect effect (AIE) in the model. The ADE is turned off by removing the mass of aerosol species from the calculation of aerosol optical properties as did in Qiu et al. (2017). The AIE is turned off by using a prescribed vertically uniform cloud droplet number, which is calculated from the CTL case during the whole simulation period, following Gao et al. (2015) and Zhang et al., (2015a). The differences between CTL and NoARE (i.e., CTL minus NoARE) represent the impacts of aerosol radiative forcing.

The IPR analysis method is applied to all the designed experiments. Comparing the contributions of each detailed

9

process between pollution accumulation stage and dissipation stage in CTL can quantitatively explain the reason for the variation of the $PM_{2.5}$ concentrations in BTH. Meanwhile, the prominent physical or chemical process responsible for the aerosol radiative impacts on the haze episode can also be investigated by analyzing the IPR analysis method used in CTL and NoARE cases.

5   All the five simulations are conducted for the period from 13 to 29 December 2015, and the initial three days are discarded as the model spin-up to minimize the impacts of initial conditions. Simulation results from the CTL case during 16 to 29 December 2015 are used to evaluate the model performance.

2.4 Observational data

Simulated meteorological parameters in CTL case, including 2 m temperature (T_2), 2 m relative humidity (RH_2), 10 m
10   wind speed (WS_{10}) and 10 m wind direction (WD_{10}), are compared with hourly observations at twelve stations, which are collected from NOAA's National Climatic Data Center (https://gis.ncdc.noaa.gov/maps/ncei/cdo/hourly). Due to limited observations of PBL height in BTH, the retrieved PBLH in 3-hour intervals obtained from the GDAS (Global Data Assimilation System) (https://ready.arl.noaa.gov/READYamet.php) in Beijing (39.93 °N, 116.28 °E) is also used to evaluate the model performance. More detailed information about the GDAS meteorological dataset (1 °×1 °) can be found in Rolph et
15   al. (2013), Kong et al. (2015) and https://www.ready.noaa.gov/gdas1.php. Hourly shortwave downward radiation flux (SWDOWN) at the Xianghe station (39.75 °N, 116.96 °E) is taken from WRMC-BSRN (World Radiation Monitoring Center-Baseline Surface Radiation Network, http://bsrn.awi.de) for the energy budget evaluation. The hourly observed surface-layer $PM_{2.5}$ concentrations at the 59 stations are obtained from the CNEMC (China National Environmental Monitoring Center, http://www.cnemc.cn/). The daily measurements of mass concentrations of SO_4^{2-}, NO_3^-, NH_4^+, BC and
20   OC are collected at the sites of (39.97 °N, 116.37 °E) in Beijing and (38.03 °N, 114.53 °E) in Shijiazhuang (Huang et al., 2017; Liu et al., 2018). Detailed locations of these observations are shown in Fig. 1(b).

3. Model evaluation

Accurate representations of observed meteorological fields and pollutant concentrations provide foundations for haze

analysis with the WRF-Chem model. Detailed comparisons between observed and simulated meteorological parameters (T_2, RH_2, WS_{10}, WD_{10}, PBLH, and SWDOWN) and pollutant concentrations ($PM_{2.5}$, BC, OC, SO_4^{2-}, NO_3^-, and NH_4^+) are presented in this section.

3.1 Meteorological parameters

5   Figure 2 shows the time series of observed and simulated hourly meteorological variables averaged over the 12 stations during 16-29 December 2015. Corresponding statistical metrics, including mean value, normalized mean bias (NMB), mean fractional bias (MFB), mean fractional error (MFE), index of agreement (IOA), and correlation coefficient (R) are presented in Table 3. As shown in Fig. 2, simulated T_2, RH_2, WS_{10} and WD_{10} agree well with the observational data. For temperature, the WRF-Chem model can perfectly depict its diurnal and daily variations with R and IOA of 0.90 and 0.94, respectively, but

10   slightly overestimates the low values at night, with the NMB of 1%. Observed relative humidity can be reasonably reproduced by the model with R and IOA of 0.73 and 0.82, respectively. But a persistent underestimation is found with the NMB of −12%. Different surface layer and boundary layer parameterizations may have influence on the simulated near-surface moisture fluxes, and the settings of these schemes can partially explain the biases of RH_2 between observations and simulations (Qian et al., 2016). This negative bias of RH_2 can also be simulated by other studies (Zhang et al., 2009; Gao

15   et al., 2015). WRF-Chem can capture the observed low values of wind speed during 19-23 December and high values of wind speed during 16-17 and 25-27 December. The positive NMB of 28% may probably result from unresolved topographical features in surface drag parameterization and the coarse resolution used in the nested domain (Yahya et al., 2015; Zheng et al., 2015). For wind direction, the calculated NMB is 1% and the IOA is 0.65, indicating that the WRF-Chem model can generally reproduce the varied wind direction during the simulation period.

20   Simulated hourly PBLH and SWDOWN are also compared with observations in Fig. 3. It is noted that PBLH provided by GDAS of NOAA are in 3-hour intervals. The simulations in CTL case agree well with the observations, including capturing the daily maximum in the daytime and the low values at night. The correlation coefficients are 0.68 and 0.91 for PBLH and SWDOWN, respectively.

3.2 PM$_{2.5}$ and its components

Observed hourly surface-layer PM$_{2.5}$ concentrations from 16 to 29 December 2015 in the nine cities (Shengyang, Beijing, Xingtai, Hengshui, Baoding, Langfang, Yangquan, Anyang, and Jinan) are compared with the model results from CTL case (Fig. 4). The statistical metrics are shown in Table 3. Generally, WRF-Chem model can reasonably reproduce the evolutional characteristics of the observed PM$_{2.5}$ concentrations in the nine cities (Rs=0.57-0.90). Both the observed and simulated PM$_{2.5}$ concentrations exhibit a growth trend during December 16-22 and 28-29, and a decreasing tendency during December 23-27. However, an obvious underestimation is found in Beijing from 25 to 26 December when a maximum hourly concentration of 600 μg m^{-3} was observed. This negative bias is also simulated by previous studies (Chen et al., 2018; Zhang et al., 2018b), and the possible reasons for the underestimation are (1) the bias in simulated meteorological conditions (e.g., underestimated RH$_2$ and overestimated WS$_{10}$); (2) the missing mechanisms of some gas-aerosol phase partitioning and heterogeneous reactions which may produce secondary inorganic aerosol (Huang et al., 2014a; Wang et al., 2014); (3) the lack of SOA simulation in MOSAIC mechanism (Gao et al., 2016). Generally, the performance statistics of PM$_{2.5}$ in almost all cities meet the model performance goal (MFB within ±30% and MFE≤50%) proposed by Boylan and Russel (2006).

Figure 5 compares the simulated and observed surface-layer concentrations of BC, OC, SO$_4^{2-}$, NO$_3^-$, and NH$_4^+$ in Beijing and Shijiazhuang averaged during 16-29 December 2015. WRF-Chem model underestimates the concentrations of SO$_4^{2-}$, NH$_4^+$ and OC in Beijing (Shijiazhuang) by 19% (40%), 14% (9%), and 21% (41%), respectively, but overestimates the NO$_3^-$ concentration by 29% (44%). Due to the low reactivity of BC in the atmosphere, the uncertainty in BC emission may cause the biases in Beijing (NMB=+10%) and Shijiazhuang (NMB=-24%). For OC, the underestimation may result from the lack of SOA in the MOSAIC aerosol module (Qiu et al., 2017). Missing some mechanisms of SO$_2$ gas-phase and aqueous-phase oxidation, as well as heterogeneous chemistry may explain the underestimation of SO$_4^{2-}$. It is noted that similar biases of aerosol components were also reported by other WRF-Chem studies (Zhang et al., 2015a; Qiu et al., 2017).

4. Formation and evolution mechanisms of the haze episode

In this section, we first reproduce the evolution of the severe haze episode, and then investigate the formation and

evolution mechanisms, including examining contributions of local emission and regional transport to the $PM_{2.5}$ concentration in BTH, and the contributions of each detailed physical/chemical process to the variations in the $PM_{2.5}$ concentration.

4.1 Spatial-temporal evolutions of surface-layer $PM_{2.5}$ concentrations

Figures 6(a-k) show the spatial distributions of simulated daily mean surface-layer $PM_{2.5}$ concentrations from 17 to 28 December 2015. From December 17, aerosol particles started to accumulate in the near-surface layer in BTH under a prevailing southerly air flow. On December 20, the BTH region was under a uniform pressure field (Fig. S2(a)). The regional average wind speed was less than 3 m s^{-1}, and the boundary layer became stable, which constrained aerosols within a low mixing layer. Meanwhile, a low-pressure center situated to the north of BTH, where air pollutants from south, southwest, and southeast converged. Consequently, the daily mean $PM_{2.5}$ concentration averaged over BTH was over 200 μg m^{-3}. On December 21, a weak low-pressure center was formed near the Bohai Bay and a weak high-pressure center moved to Shandong Peninsula (Fig. S2(b)). The synoptic conditions brought more air masses from south to north, and worsened air quality in BTH. On December 22, a weak high pressure system moved within Inner Mongolia (Fig. S2(c)), which could bring cold air to the BTH region. Meanwhile, the polluted air could also be transported back to the BTH, leading to a continuous increase in the $PM_{2.5}$ concentration, with the maximum daily mean value exceeding 600 μg m^{-3} in BTH (Fig. 6(e)). Due to the enhanced anticyclone originated from Siberian (Fig. S2(d)), the accumulation of aerosol particles in BTH was terminated with the incursion of a strong cold front from 23 to 27 December. But frequent transitions between high and low pressure systems over BTH accompanying with the shifting wind directions resulted in a quick $PM_{2.5}$ variation, especially on December 24 and 25, when a low-pressure system developed northeast of BTH (Fig. S2(e)). The air mass in BTH was influenced by the pollutants from south, resulting in a temporary increase in the concentration of $PM_{2.5}$ on December 25. After December 27, another haze episode gradually formed.

According to the trends in simulated $PM_{2.5}$ concentrations averaged over the BTH region (Fig. 6(l)), we divide the whole simulation period into three stages: (1) aerosol accumulation stage (December 16-22, Stage_1); (2) aerosol dispersion stage (December 23-27, Stage_2); (3) formation stage for another haze event (December 28-29, Stage_3). In this manuscript, we mainly focus on the first two stages to reveal important factors that cause the accumulation and dispersion of particulate

matters.

In Stage_1, the daily mean $PM_{2.5}$ concentrations averaged over BTH increased from 24.2 μg m^{-3} to 289.8 μg m^{-3}, and the average $PM_{2.5}$ concentration was 145.6 μg m^{-3} (Fig. 7(a)), close to the air quality threshold value of "heavily polluted" ($PM_{2.5}$ 24-h average concentration > 150 μg m^{-3}). The WS_{10} was low (Fig. 7(b)), especially during the heavy pollution period (20-22 December), and the mean wind speed was 2.3 m s^{-1}, less than 3.2 m s^{-1} (one of the indicators used to define air stagnation by NOAA, https://www.ncdc.noaa.gov/societal-impacts/air-stagnation/overview), indicating that the near surface circulation was insufficient to disperse accumulated air pollutants. The decreased PBLH (from 701.6 m to 109.9 m) could compress air pollutants into a shallow layer, resulting in an elevated pollution level. During Stage_2, the $PM_{2.5}$ concentration decreased gradually with the increased wind speed and PBLH. The $PM_{2.5}$ concentration averaged during Stage_2 was 107.9 μg m^{-3}, still exceeding the Grade II standard (75 μg m^{-3}) defined by the National Ambient Air Quality Standards of China.

4.2 Contributions of local emission and regional transport to $PM_{2.5}$ concentrations

Previous studies have reported that anthropogenic emission was the dominant cause of haze events in China (Jiang et al., 2013; Sun et al., 2014; Gu and Liao, 2016; Yang et al., 2016b). Emission control measures have been taken to ensure good air quality for major events (e.g., APEC) or to mitigate the severity of coming pollution episodes (Zhou et al., 2018). Other studies, such as Sun et al. (2017) and Wang et al. (2017), pointed out that regional transport contributed more than 50% of the particulate concentrations in BTH during haze events. This section discusses the contributions of local anthropogenic emission and regional transport to the $PM_{2.5}$ concentration in BTH, aiming to reveal the relative importance during this haze episode.

As shown in Fig. 7(a), the $PM_{2.5}$ concentration in BTH during Stage_1 was mainly contributed by the combined effects of local emission and regional transport. The contributions of local emission and regional transport to the $PM_{2.5}$ concentration were comparable (49% and 32%, respectively), especially during the heavy pollution period (December 20-22, 43% vs. 37%). During Stage_2, the contributions of regional transport decreased from 30% to 16%. The relative high $PM_{2.5}$ concentration (107.9 μg m^{-3}) was principally caused by the local emission. On average, the contributions of local emission and regional transport to the $PM_{2.5}$ concentration in Stage_2 were 51% and 24%, respectively. The impact of regional

transport could be qualitatively expressed by specific humidity, which was treated as an indicator for the origin of air masses (Jia et al., 2008). Air masses from the south were usually warmer and wetter than those from the north, so the specific humidity averaged over the BTH was higher in Stage_1 (1.7 g/kg) than that in Stage_2 (1.4 g/kg) (Fig. 7(b)). The evolution of $PM_{2.5}$ nicely followed the trend of specific humidity with a high correlation coefficient of 0.86.

4.3 Contributions of each physical/chemical process to variations in $PM_{2.5}$ concentrations

Figures 8(a1-a2) show the diurnal variations of $PM_{2.5}$ concentrations averaged over the BTH region during Stage_1 and Stage_2, respectively. The $PM_{2.5}$ concentration increased by 43.9 μg m^{-3} (from 136.5 μg m^{-3} at 00:00LST to 180.4 μg m^{-3} at 23:00LST) during the period of particulate accumulation (Stage_1), but it decreased by 41.5 μg m^{-3} during the period of particulate elimination (Stage_2).

The hourly $PM_{2.5}$ changes induced by each and all physical/chemical processes during Stage_1 and Stage_2 by using the IPR analysis method are shown in Figs. 8(b1-b2). During both stages, the dominant sources of surface-layer $PM_{2.5}$ were EMIS and AERC, while the main sinks were TRAN, DIFF, and DRYD. The maximum positive contribution of EMIS could be found during the rush hours (07:00-08:00LST and 16:00-19:00LST) (Fig. S3). The maximum negative contributions of TRAN and DIFF appeared at late night (01:00-05:00LST) and at noon (11:00-14:00LST), respectively.

To explain the reason for 24-h $PM_{2.5}$ increase during Stage_1 and 24-h $PM_{2.5}$ decrease during Stage_2 (Figs. 8(a1-a2)), we quantify the contributions of each physical/chemical process to 24-h $PM_{2.5}$ changes for both stages (Figs. 8(c1-c2)), which are calculated by integrating hourly $PM_{2.5}$ changes induced by each process from 00:00LST to 23:00LST (Figs. 8(b1-b2)). In WRF-Chem, DRYD is intermingled with vertical diffusion, so changes in the column burden during vertical mixing can be attributed to DRYD (Tao et al., 2015). Following Tao et al. (2015), we define vertical mixing (VMIX) as the sum of DIFF and DRYD. As shown in Figs. 8(c1-c2), contributions of AERC, TRAN and VMIX processes to 24-h $PM_{2.5}$ changes were +29.6 (+17.9) μg m^{-3}, -71.8 (-103.6) μg m^{-3} and -177.3 (-221.6) μg m^{-3} for Stage_1 (Stage_2), respectively. Small differences were found for contributions from other processes between Stage_1 and Stage_2 (differences smaller than 5 μg m^{-3}). Therefore, the $PM_{2.5}$ increase over the BTH region during haze formation stage was mainly attributed to strong production by aerosol chemistry process and weak removal by advection and vertical mixing processes. On the contrary,

during haze elimination stage (Stage_2), more aerosols in BTH were transported out of BTH or dispersed to the upper atmosphere or subsided to the ground. What's more, the dry cold air from the north decreased the specific humidity (as shown in Fig. 7(b)) in BTH, leading to weaker production of secondary aerosols by aerosol chemistry process.

5 Aerosol radiative effects (ARE) on the haze episode

Previous studies have demonstrated that the aerosol radiative forcing could increase the near-surface $PM_{2.5}$ concentrations by about 12%-29% (Gao et al., 2015; Gao et al., 2016; Qiu et al., 2017; Zhou et al., 2018). However, the detailed influence mechanisms (i.e., the prominent physical or chemical process responsible for the aerosol radiative impacts on $PM_{2.5}$ concentrations) are still unclear. In this section, we examine the effects of aerosol radiative forcing on meteorological parameters and $PM_{2.5}$ levels during the haze episode, with a special focus on the detailed influence mechanism by using the IPR analysis.

5.1 Effects of aerosol radiative forcing on meteorological parameters and $PM_{2.5}$ concentrations

Figure 9 illustrates the impacts of aerosols on the downward shortwave radiative flux (SW) at the surface (BOT_SW) and in the atmosphere (ATM_SW), calculated by subtracting the model results of NoARE from those of CTL, during Stage_1, Stage_2, and the whole simulation period. Downward SW at the surface was strongly decreased when ARE was considered, especially over high aerosol-loading regions during heavily polluted periods. Generally, the shortwave radiation fluxes at the surface averaged over BTH were reduced by 28% (23.9 W m^{-2}) in Stage_1, 18% (16.6 W m^{-2}) in Stage_2, and 23% (19.9 W m^{-2}) during the whole simulation period, respectively. Contrary to the significant negative effects at the surface, as a result of ARE, the downward SW fluxes in the atmosphere averaged over BTH were increased by 65% (19.1 W m^{-2}) in Stage_1, 37% (10.8 W m^{-2}) in Stage_2, and 51% (14.7 W m^{-2}) during the whole period, respectively.

The impacts of ARE (including aerosol direct and indirect effects) on meteorological parameters and $PM_{2.5}$ concentrations are analyzed in Fig. 10. Because less SW could reach the ground, near-surface temperature was decreased over BTH (Fig. 10(a)), especially during heavy pollution periods, and the largest decrease was up to 2 k. Meanwhile, the increased SW in the atmosphere could warm the upper air. As a result, a more stable atmosphere was expected. It is known

that the atmospheric stability can be exactly characterized by the profile of equivalent potential temperature (EPT) (Bolton, 1980; Zhao et al., 2013; Yang et al., 2016a). If EPT rises with height, the atmosphere is stable. As shown in Fig. 10(b), the EPT was decreased in the lower atmosphere (below ~1000 m) with the largest decrease of 3 k on December 22, but increased in the upper atmosphere (above ~1200 m). The change in the EPT profile indicated that ARE could lead to a more stable atmosphere, which further weakened vertical movement in BTH (Fig. 10(c)). As a result of ARE, the PBLH was decreased and the relative humidity in the lower atmosphere was increased (Fig. 10(d)). All the changes in meteorological variables were beneficial for $PM_{2.5}$ accumulation in the lower atmosphere (Fig. 10(e)). The daily maximum increase of $PM_{2.5}$ concentration was 43.2 µg m^{-3} due to ARE. It was noticed that ARE had a negative impact on the near-surface $PM_{2.5}$ concentrations during December 23-24, which could be explained that absorbing aerosols (i.e., BC) induced anomalous northeasterlies, and the relatively clean air transported from the northeastern regions to BTH (Fig. S4).

5.2 Influence mechanism of aerosol radiative effects

Since variations in $PM_{2.5}$ concentrations are directly caused by physical and chemical processes (Zhu et al., 2015), the IPR method is then used to investigate the detailed influence mechanisms (i.e., the prominent physical or chemical processes responsible for the aerosol radiative impacts on haze episodes). Figs. 11(a-b) show the diurnal variations of $PM_{2.5}$ concentrations in NoARE and CTL cases averaged over the BTH region in Stage_1. A 24-h increase of 39.1 µg m^{-3} was simulated in NoARE case. When aerosol radiative forcing was considered, the 24-h increase of $PM_{2.5}$ concentration was 43.9 µg m^{-3}. The enhancement of 4.8 µg m^{-3} (12%) induced by ARE could be mainly attributed to the contributions of VMIX, TRAN, and AERC processes, as shown in Fig. 11(c). The vertical mixing was strongly restrained by ARE, therefore fewer particles diffused from the surface to the upper layer, resulting in the accumulation of $PM_{2.5}$ in a lower atmospheric boundary layer. The changes induced by ARE in contributions of VMIX process exhibited positive values in the lower layers and negative values in the upper layers (Fig. S5(a)). Generally, the VMIX process contributed +22.5 µg m^{-3} to the enhancement in 24-h $PM_{2.5}$ increase (+4.8 µg m^{-3}) for Stage_1. The TRAN process, however, contributed -19.6 µg m^{-3}. Constrained vertical mixing due to ARE could increase aerosol precursors and water vapor in the thin boundary layer to enhance the formation of secondary particles. Generally, the AERC process contributed +1.2 µg m^{-3}. The positive contribution of AERC

17

was mainly distributed over the high polluted regions in BTH (Fig. S5(b)). Detailedly, the average changes in concentrations of SO_4^{2-}, NO_3^-, and NH_4^+ during the daytime from 11:00 to 17:00LST in Stage_1 were -0.5 μg m^{-3}, +1.3 μg m^{-3}, and +0.8 μg m^{-3}, respectively. The decreased near-surface temperature caused by ARE may suppress the chemical formation of SO_4^{2-}. Generally, the total contribution of VMIX, TRAN, and AERC processes to the change in 24-h PM$_{2.5}$ increase caused by ARE was +4.1 μg m^{-3}, and the restrained vertical mixing could be the primary reason for near-surface PM$_{2.5}$ increase when aerosol radiative forcing was considered.

Figure 12(a) shows the vertical profiles of the 24-h increases in PM$_{2.5}$ concentrations (23:00LST minus 00:00LST) averaged over BTH during Stage_1 in CTL and NoARE cases. Below ~300 m (between L01 and L04), the 24-h increase simulated by CTL was larger than that in NoARE, which could be mainly explained by that the positive contributions of VMIX exceeded the negative contributions of TRAN in the lower atmosphere when aerosol radiative effect was considered (Fig. 12(b)). However, in the upper layers (from 300 to 2000 m), aerosol radiative forcing weakened the 24-h PM$_{2.5}$ increase during Stage_1. When aerosol radiative effect was considered, fewer particulate matters, precursors and water vapor were diffused from the surface to the upper layers, and therefore fewer particles were formed in the upper layers. Despite of the positive contributions of TRAN, the net contributions of VMIX, TRAN, and AERC to PM$_{2.5}$ changes caused by ARE in the upper atmosphere were negative.

6. Conclusions and discussions

In this study, an online coupled mesoscale meteorology-chemistry model (WRF-Chem) with an improved integrated process rate (IPR) analysis (i.e., process analysis) scheme is applied to investigate the formation and evolution mechanisms of a severe haze episode happened in the BTH region during 16-29 December 2015. Sensitivity experiments are conducted to examine the contributions of local emission and regional transport to the PM$_{2.5}$ concentrations during the haze event, while IPR analysis is used to quantify the contributions of each physical/chemical process to the variation in PM$_{2.5}$ concentration. The impacts of aerosol radiative forcing (including direct and indirect effects) are also quantified, with a special focus on the detailed influence mechanism (i.e., prominent process responsible for the aerosol radiative impacts on the haze event). An integrated comparison between observations and simulations demonstrates good performance for both meteorological and

chemical variables, indicating that the WRF-Chem model has the capability to reproduce the haze episode.

Spatial-temporal evolutions of the near-surface $PM_{2.5}$ concentration, and the contributions of local emission and regional transport to the severe haze even in BTH, were firstly analyzed. During the aerosol accumulation stage (December 16-22, Stage_1), the daily $PM_{2.5}$ concentration in BTH experienced a consistent increase, with the mean value of 145.6 μg m^{-3}. The contributions of local emission and regional transport to the $PM_{2.5}$ concentration were comparable (49% and 32%, respectively), meaning the combined effect resulted in the high $PM_{2.5}$ concentration in BTH. During the aerosol dispersion stage (December 23-27, Stage_2), the average $PM_{2.5}$ concentration in BTH was 107.9 μg m^{-3}. The contributions of local emission and regional transport were 51% and 24%, respectively. Therefore, the relatively high $PM_{2.5}$ concentration during Stage_2 was principally caused by local emission. During December 28-29 (Stage_3), another haze event was formed and developed.

The IPR analysis was then used to explain the reason for $PM_{2.5}$ increase during Stage_1 and decrease during Stage_2, by quantifying the contributions of each physical/chemical process to variations in $PM_{2.5}$ concentration. During both stages, the dominant sources were emission (EMIS) and aerosol chemistry (AERC), while the main sinks were turbulent diffusion (DIFF), advection (TRAN), and dry deposition (DRYD). The $PM_{2.5}$ concentration increased by 43.9 μg m^{-3} (23:00LST minus 00:00LST) during Stage_1, but it decreased by 41.5 μg m^{-3} during Stage_2. Contributions of AERC, TRAN and VMIX (vertical mixing, the sum of DRYD and DIFF) to the 24-h $PM_{2.5}$ changes were +29.6 (+17.9) μg m^{-3}, -71.8 (-103.6) μg m^{-3} and -177.3 (-221.6) μg m^{-3} for Stage_1 (Stage_2), respectively. Small differences in contributions from other processes were found between Stage_1 and Stage_2. Therefore, the $PM_{2.5}$ increase over BTH during the haze formation stage was attributed to strong production by aerosol chemistry process and weak removal by advection and vertical mixing processes.

When aerosol radiative forcing was considered, the equivalent potential temperature was decreased in the lower layers but increased in the upper layers, leading to a more stable atmosphere. Meanwhile, the decreased PBLH and increased relative humidity were also beneficial for $PM_{2.5}$ accumulation. The daily maximum increase of the near-surface $PM_{2.5}$ concentration in BTH was 43.2 μg m^{-3}. The IPR method was also used to investigate the detailed influence mechanism of aerosol radiative effects. When aerosol radiative feedback was considered, the 24-h $PM_{2.5}$ increase was enhanced by 4.8 μg

19

m^{-3} (12%) during Stage_1, which could be mainly attributed to the contributions of VMIX (+22.5 μg m^{-3}), TRAN (-19.6 μg m^{-3}), and AERC (+1.2 μg m^{-3}). The restrained vertical mixing could be the primary reason for near-surface PM$_{2.5}$ increase when aerosol radiative forcing was considered.

There are some limitations in this work. The uncertainty of the MIX anthropogenic emission inventory, the lack of secondary organic aerosols, and the missing mechanisms of some heterogeneous reactions may result in large uncertainties in the final simulation results, especially the predicted aerosol chemical compositions, such as SO_4^{2-}, NO_3^- and NH_4^+. The biases in simulated concentrations of SO_4^{2-}, NO_3^- and NH_4^+ may have impacts on the contributions of AERC and CLDC processes to the air pollution variation. Uncertainties should be quantitatively analyzed in future studies. Besides, conclusions draw from a case study in BTH cannot represent a full view of the underlying mechanisms of haze formation and elimination. Better understanding will be attained by conducting multiple-case simulations in future. What's more, an anomalous northeasterly induced by absorbing aerosols was observed, leading to a decrease in the near-surface PM$_{2.5}$ concentrations during December 23-24 2015 in BTH, which was different from previous studies that reported light-absorbing aerosols could worsen air quality (Li et al., 2016; Huang et al., 2018; Gao et al., 2018). More experiments should be designed in future to examine the changes in atmospheric thermal and atmospheric dynamic caused by absorbing aerosol radiative forcing and their impacts on haze episodes.

As Zheng et al. (2018) pointed out that the PM$_{2.5}$ concentration in China has been decreasing in recent years, but the decreased fine particulate matter could stimulate ozone production (Li et al., 2019a; Zhu et al., 2019). Multi-pollutant mixture may be a hot topic in the future, and the IPR analysis can be a useful method to provide a quantitative analysis about the formation mechanism of the complex air pollutions, including figuring out the major physical/chemical process behind these events. Meanwhile, significant differences between model predictions (e.g., O$_3$ and PM$_{2.5}$) are found among current multi-scale air quality models (Chen et al., 2019b; Li et al., 2019b), even though the same inputs are used. These different performances can be associated with the differences in model formulations, including parameterizations and numerical methods (Carmichael et al., 2008). In order to acquire a quantitative attribution of the cause of differences between simulation results, process analysis method should be developed and implemented in these models, and the IPR analysis will be easier to draw conclusions about the fundamental problems that cause the differences between model predictions.

Data availability

Observational datasets and simulation results are available upon request to the corresponding author (hongliao@nuist.edu.cn).

Author contributions

HL and LC conceived the study and designed the experiments. LC and JZ performed the simulations and carried out the data analysis. YG, MZ, YQ, ZL, NL and YW provided useful comments on the paper. LC prepared the manuscript with contributions from all co-authors.

Competing interests

The authors declare that they have no conflict of interest.

Special issue statement

This study is part of the special issue "Regional transport and transformation of air pollution in eastern China". It is not associated with a conference.

Acknowledgements

References

Ackermann, I. J., Hass, H., Memmesheimer, M., Ebel, A., Binkowski, F. S., and Shankar, U. M. A.: Modal aerosol dynamics model for Europe: Development and first applications. Atmospheric environment, 32(17), 2981-2999, 10.1016/S1352-2310(98)00006-5, 1998.

Barnard, J. C., Fast, J. D., Paredes-Miranda, G., Arnott, W. P., and Laskin, A.: Technical Note: Evaluation of the WRF-Chem "Aerosol Chemical to Aerosol Optical Properties" Module using data from the MILAGRO campaign, Atmospheric Chemistry and Physics, 10, 7325-7340, 10.5194/acp-10-7325-2010, 2010.

Bolton, D.: The computation of equivalent potential temperature. Monthly Weather Review, 108, 1046-1053, 10.1175/1520-0493(1980)108<1046:TCOEPT>2.0.CO;2, 1980.

Boylan, J. W., and Russell, A. G.: PM and light extinction model performance metrics, goals, and criteria for three-dimensional air quality models, Atmospheric Environment, 40, 4946-4959, 10.1016/j.atmosenv.2005.09.087, 2006.

Chen, D., Liu, Z., Fast, J., and Ban, J.: Simulations of sulfate-nitrate-ammonium (SNA) aerosols during the extreme haze events over northern China in October 2014, Atmospheric Chemistry and Physics, 16, 10707-10724, 10.5194/acp-16-10707-2016, 2016.

Chen, L., Zhang, M., Zhu, J., Wang, Y., and Skorokhod, A.: Modeling Impacts of Urbanization and Urban Heat Island Mitigation on Boundary Layer Meteorology and Air Quality in Beijing Under Different Weather Conditions, Journal of Geophysical Research: Atmospheres, 123, 4323-4344, 10.1002/2017jd027501, 2018.

Chen, L., Gao, Y., Zhang, M., Fu, J. S., Zhu, J., Liao, H., Li, J., Huang, K., Ge, B., Wang, X., LAM, Y. F., Lin, C. Y., Itahashi, S., Nagashima, T., Kajino, M., Yamaji, K., Wang, Z., and Kurokawa, J.-I.: MICS-Asia III: Multi-model comparison and evaluation of aerosol over East Asia, Atmos. Chem. Phys. Discuss., 10.5194/acp-2018-1346, in review, 2019.

Chen, J., Li, Z., Lv, M., Wang, Y., Wang, W., Zhang, Y., Wang, H., Yan, X., Sun, Y., and Cribb, M.: Aerosol hygroscopic growth, contributing factors, and impact on haze events in a severely polluted region in northern China, Atmos. Chem. Phys., 19, 1327-1342, 10.5194/acp-19-1327-2019, 2019.

Ding, A. J., Huang, X., Nie, W., Sun, J. N., Kerminen, V. M., Petäjä, T., Su, H., Cheng, Y. F., Yang, X. Q., Wang, M. H., Chi, X. G., Wang, J. P., Virkkula, A., Guo, W. D., Yuan, J., Wang, S. Y., Zhang, R. J., Wu, Y. F., Song, Y., Zhu, T., Zilitinkevich, S., Kulmala, M., and Fu, C. B.: Enhanced haze pollution by black carbon in megacities in China, Geophysical Research Letters, 43, 2873-2879, 10.1002/2016gl067745, 2016.

Emmons, L. K., Walters, S., Hess, P. G., Lamarque, J.-F., Pfister, G. G., Fillmore, D., Granier, C., Guenther, A., Kinnison, D., Laepple, T., Orlando, J., Tie, X., Tyndall, G., Wiedinmyer, C., Baughcum, S. L., and Kloster, S.: Description and evaluation of the Model for Ozone and Related chemical Tracers, version 4 (MOZART-4), Geosci. Model Dev., 3, 43-67, 10.5194/gmd3-43-2010, 2010.

Gao, Y., Zhang, M., Liu, Z., Wang, L., Wang, P., Xia, X., Tao, M., and Zhu, L.: Modeling the feedback between aerosol and meteorological variables in the atmospheric boundary layer during a severe fog-haze event over the North China Plain, Atmospheric Chemistry and Physics, 15, 4279-4295, 10.5194/acp-15-4279-2015, 2015.

Gao, M., Carmichael, G. R., Wang, Y., Saide, P. E., Yu, M., Xin, J., Liu, Z., and Wang, Z.: Modeling study of the 2010 regional haze event in the North China Plain, Atmospheric Chemistry and Physics, 16, 1673-1691, 10.5194/acp-16-1673-2016, 2016.

Gao, J., Zhu, B., Xiao, H., Kang, H., Pan, C., Wang, D., and Wang, H.: Effects of black carbon and boundary layer interaction on surface ozone in Nanjing, China, Atmospheric Chemistry and Physics, 18, 7081-7094, 10.5194/acp-18-7081-2018, 2018.

Gipson, G. L.: Science algorithms of the EPA Models-3 community multiscale air quality (CMAQ) modeling system: process analysis, 37 pp., 1999.

Gonçalves, M., Jiménez-Guerrero, P., and Baldasano, J. M.: Contribution of atmospheric processes affecting the dynamics of air pollution in South-Western Europe during a typical summertime photochemical episode, Atmos. Chem. Phys., 9, 849-864, 10.5194/acp-9-849-2009, 2009.

Gong, S. L., Barrie, L. A., and Blanchet, J. P.: Modeling sea-salt aerosols in the atmosphere: 1. Model development, Journal of Geophysical Research: Atmospheres, 102, 3805-3818, 10.1029/96jd02953, 1997.

Grell, G. A., Peckham, S. E., Schmitz, R., McKeen, S. A., Frost, G., Skamarock, W. C., and Eder, B.: Fully coupled "online"

chemistry within the WRF model, Atmospheric Environment, 39, 6957-6975, 10.1016/j.atmosenv.2005.04.027, 2005.

Gu, Y.-X., and Liao, H.: Response of fine particulate matter to reductions in anthropogenic emissions in Beijing during the 2014 Asia-Pacific Economic Cooperation summit, Atmospheric and Oceanic Science Letters, 9, 411-419, 10.1080/16742834.2016.1230465, 2016.

5 Guenther, C. C.: Estimates of global terrestrial isoprene emissions using MEGAN (Model of Emissions of Gases and Aerosols from Nature). Atmospheric Chemistry and Physics, 6, www.atmos-chem-phys.net/6/3181/2006, 2006.

Guo, H., Cheng, T., Gu, X., Wang, Y., Chen, H., Bao, F., Shi, S., Xu, B., Wang, W., Zuo, X., Zhang, X., and Meng, C.: Assessment of PM2.5 concentrations and exposure throughout China using ground observations, The Science of the total environment, 601-602, 1024-1030, 10.1016/j.scitotenv.2017.05.263, 2017.

10 Han, X., Zhang, M., Gao, J., Wang, S., and Chai, F.: Modeling analysis of the seasonal characteristics of haze formation in Beijing, Atmospheric Chemistry and Physics, 14, 10231-10248, 10.5194/acp-14-10231-2014, 2014.

Han, T., Liu, X., Zhang, Y., Qu, Y., Zeng, L., Hu, M., and Zhu, T.: Role of secondary aerosols in haze formation in summer in the Megacity Beijing, Journal of environmental sciences, 31, 51-60, 10.1016/j.jes.2014.08.026, 2015.

Hu, J., Zhang, H., Chen, S., Ying, Q., Wiedinmyer, C., Vandenberghe, F., and Kleeman, M.: Identifying $PM_{2.5}$ and $PM_{0.1}$
15   Sources for Epidemiological Studies in California, Environ. Sci. Technol., 48 (9), 4980−4990, 10.1021/es404810z, 2014.

Huang, Y., Dickinson, R. E., and Chameides, W. L.: Impact of aerosol indirect effect on surface temperature over East Asia, Proceedings of the National Academy of Sciences of the United States of America, 103, 4371-4376, 10.1073/pnas.0504428103, 2006.

20 Huang, X., Song, Y., Zhao, C., Li, M., Zhu, T., Zhang, Q., and Zhang, X.: Pathways of sulfate enhancement by natural and anthropogenic mineral aerosols in China, J. Geophys. Res.-Atmos., 119, 14165-14179, 10.1002/2014JD022301, 2014a.

Huang, R. J., Zhang, Y., Bozzetti, C., Ho, K. F., Cao, J. J., Han, Y., Daellenbach, K. R., Slowik, J. G., Platt, S. M., Canonaco, F., Zotter, P., Wolf, R., Pieber, S. M., Bruns, E. A., Crippa, M., Ciarelli, G., Piazzalunga, A., Schwikowski, M., Abbaszade, G., Schnelle-Kreis, J., Zimmermann, R., An, Z., Szidat, S., Baltensperger, U., El Haddad, I., and Prevot, A.
25   S.: High secondary aerosol contribution to particulate pollution during haze events in China, Nature, 514, 218-222, 10.1038/nature13774, 2014b.

Huang, X., Liu, Z., Liu, J., Hu, B., Wen, T., Tang, G., Zhang, J., Wu, F., Ji, D., Wang, L., and Wang, Y.: Chemical characterization and source identification of PM2.5 at multiple sites in the Beijing–Tianjin–Hebei region, China, Atmos. Chem. Phys., 17, 12941-12962, 10.5194/acp-17-12941-2017, 2017.

30 Huang, X., Wang, Z., and Ding, A.: Impact of Aerosol-PBL Interaction on Haze Pollution: Multiyear Observational Evidences in North China, Geophysical Research Letters, 10.1029/2018gl079239, 2018.

IPCC: Climate Change 2013: The Physical Science Basis: Summary for Policymakers, Cambridge, UK, 2013.

Jia, Y., Rahn, K. A., He, K., Wen, T., and Wang, Y.: A novel technique for quantifying the regional component of urban aerosol solely from its sawtooth cycles, Journal of Geophysical Research, 113, 10.1029/2008jd010389, 2008.

35 Jiang, F., Zhou, P., Liu, Q., Wang, T., Zhuang, B., and Wang, X.: Modeling tropospheric ozone formation over East China in springtime, Journal of Atmospheric Chemistry, 69, 303-319, 10.1007/s10874-012-9244-3, 2012.

Jiang, H., Liao, H., Pye, H. O. T., Wu, S., Mickley, L. J., Seinfeld, J. H., and Zhang, X. Y.: Projected effect of 2000-2050 changes in climate and emissions on aerosol levels in China and associated transboundary transport, Atmospheric Chemistry and Physics, 13, 7937-7960, 10.5194/acp-13-7937-2013, 2013.

40 Jiang, C., Wang, H., Zhao, T., Li, T., and Che, H.: Modeling study of PM<sub>2.5</sub> pollutant transport across cities in China's Jing-Jin-Ji region during a severe haze episode in December 2013, Atmospheric Chemistry and Physics, 15, 5803-5814, 10.5194/acp-15-5803-2015, 2015.

Jiang, Z., Huo, F., Ma, H., Song, J., and Dai, A.: Impact of Chinese Urbanization and Aerosol Emissions on the East Asian Summer Monsoon, Journal of Climate, 30, 1019-1039, 10.1175/jcli-d-15-0593.1, 2017.

45 Kang, H., Zhu, B., Gao, J., He, Y., Wang, H., Su, J., Pan, C., Zhu, T., and Yu, B.: Potential impacts of cold frontal passage on air quality over the Yangtze River Delta, China, Atmos. Chem. Phys., 19, 3673-3685, 10.5194/acp-19-3673-2019, 2019.

Khiem, M., Ooka, R., Hayami, H., Yoshikado, H., Huang, H., and Kawamoto, Y.: Process analysis of ozone formation under different weather conditions over the Kanto region of Japan using the MM5/CMAQ modelling system, Atmospheric Environment, 44, 4463-4473, 10.1016/j.atmosenv.2010.07.038, 2010.

50 Kong, S., Li, X., Li, L., Yin, Y., Chen, K., Yuan, L., Zhang, Y., Shan, Y., and Ji, Y.: Variation of polycyclic aromatic

hydrocarbons in atmospheric PM2.5 during winter haze period around 2014 Chinese Spring Festival at Nanjing: Insights of source changes, air mass direction and firework particle injection, Sci. Total Environ., 520, 59–72, 10.1016/j.scitotenv.2015.03.001, 2015.

Lei, Y., Zhang, Q., He, K. B., and Streets, D. G.: Primary anthropogenic aerosol emission trends for China, 1990-2005, Atmospheric Chemistry and Physics, 11, 931-954, 10.5194/acp-11-931-2011, 2011.

Li, Z., Li, C., Chen, H., Tsay, S. C., Holben, B., Huang, J., Li, B., Maring, H., Qian, Y., Shi, G., Xia, X., Yin, Y., Zheng, Y., and Zhuang, G.: East Asian Studies of Tropospheric Aerosols and their Impact on Regional Climate (EAST-AIRC): An overview, Journal of Geophysical Research, 116, 10.1029/2010jd015257, 2011.

Li, Y., An, J., and Gultepe, I.: Effects of additional HONO sources on visibility over the North China Plain, Advances in Atmospheric Sciences, 31, 1221-1232, 10.1007/s00376-014-4019-1, 2014.

Li, K., Liao, H., Mao, Y., and Ridley, D. A.: Source sector and region contributions to concentration and direct radiative forcing of black carbon in China, Atmospheric Environment, 124, 351-366, 10.1016/j.atmosenv.2015.06.014, 2016.

Li, J., Du, H., Wang, Z., Sun, Y., Yang, W., Li, J., Tang, X., and Fu, P.: Rapid formation of a severe regional winter haze episode over a mega-city cluster on the North China Plain, Environmental pollution, 223, 605-615, 10.1016/j.envpol.2017.01.063, 2017a.

Li, M., Zhang, Q., Kurokawa, J.-i., Woo, J.-H., He, K., Lu, Z., Ohara, T., Song, Y., Streets, D. G., Carmichael, G. R., Cheng, Y., Hong, C., Huo, H., Jiang, X., Kang, S., Liu, F., Su, H., and Zheng, B.: MIX: a mosaic Asian anthropogenic emission inventory under the international collaboration framework of the MICS-Asia and HTAP, Atmospheric Chemistry and Physics, 17, 935-963, 10.5194/acp-17-935-2017, 2017b.

Li, Z., Rosenfeld, D., and Fan, J.: Aerosols and their impact on radiation, clouds, precipitation, and severe weather events, Oxford Research Encyclopedias, 10.1093/acrefore/9780199389414.013.126, 2017c.

Li, Z., Guo, J., Ding, A., Liao, H., Liu, J., Sun, Y., Wang, T., Xue, H., Zhang, H., and Zhu, B.: Aerosol and boundary-layer interactions and impact on air quality, Nat. Sci. Rev., 4, 810-833, 10.1093/nsr/nwx117, 2017d.

Li, K., Liao, H., Cai, W., and Yang, Y.: Attribution of Anthropogenic Influence on Atmospheric Patterns Conducive to Recent Most Severe Haze Over Eastern China, Geophysical Research Letters, 45, 2072-2081, 10.1002/2017gl076570, 2018a.

Li, N., Lu, Y., Liao, H., He, Q., Li, J., and Long, X.: WRF-Chem modeling of particulate matter in the Yangtze River Delta region: Source apportionment and its sensitivity to emission changes, PLoS ONE, 13(12):e0208944, 10.1371/journal.pone.0208944, 2018b.

Li, K., Jacob, D. J., Liao, H., Shen, L., Zhang, Q., and Bates, K. H.: Anthropogenic drivers of 2013−2017 trends in summer surface ozone in China, P. Natl. Acad. Sci. USA, 116, 422–427, 10.1073/pnas.1812168116, 2019a.

Li, J., Nagashima, T., Kong, L., Ge, B., Yamaji, K., Fu, J. S., Wang, X., Fan, Q., Itahashi, S., Lee, H.-J., Kim, C.-H., Lin, C.-Y., Zhang, M., Tao, Z., Kajino, M., Liao, H., Li, M., Woo, J.-H., Kurokawa, J.-I., Wu, Q., Akimoto, H., Carmichael, G. R., and Wang, Z.: Model evaluation and inter-comparison of surface-level ozone and relevant species in East Asia in the context of MICS-Asia phase III Part I: overview, Atmos. Chem. Phys. Discuss., 10.5194/acp-2018-1283, in review, 2019b.

Liu, Z., Gao, W., Yu, Y., Hu, B., Xin, J., Sun, Y., Wang, L., Wang, G., Bi, X., Zhang, G., Xu, H., Cong, Z., He, J., Xu, J., and Wang, Y.: Characteristics of PM2.5 mass concentrations and chemical species in urban and background areas of China: emerging results from the CARE-China network, Atmos. Chem. Phys., 18, 8849-8871, 10.5194/acp-18-8849-2018, 2018a.

Liu, Q., Jia, X., Quan, J., Li, J., Li, X., Wu, Y., Chen, D., Wang, Z., and Liu, Y.: New positive feedback mechanism between boundary layer meteorology and secondary aerosol formation during severe haze events, Scientific reports, 8, 6095, 10.1038/s41598-018-24366-3, 2018b.

Lo, J. C.-F., Yang, Z.-L., and Pielke, R. A.: Assessment of three dynamical climate downscaling methods using the Weather Research and Forecasting (WRF) model, Journal of Geophysical Research, 113, 10.1029/2007jd009216, 2008.

Lou, S., Yang, Y., Wang, H., Smith, S.J., Qian, Y., and Rasch, P.J.: Black carbon amplifies haze over the North China Plain by weakening the East Asian winter monsoon, Geophysical Research Letters, 46, 452-460, 10.1029/2018GL080941, 2019.

Otte, T. L.: The Impact of Nudging in the Meteorological Model for Retrospective Air Quality Simulations. Part I: Evaluation against National Observation Networks, Journal of Applied Meteorology and Climatology, 47, 1853-1867, 10.1175/2007jamc1790.1, 2008.

Petaja, T., Jarvi, L., Kerminen, V. M., Ding, A. J., Sun, J. N., Nie, W., Kujansuu, J., Virkkula, A., Yang, X. Q., Fu, C. B., Zilitinkevich, S., and Kulmala, M.: Enhanced air pollution via aerosol-boundary layer feedback in China, Scientific reports, 6, 18998, 10.1038/srep18998, 2016.

Qian, Y., Yan, H., Berg, L. K., Hagos, S., Feng, Z., Yang, B., and Huang, M.: Assessing Impacts of PBL and Surface Layer Schemes in Simulating the Surface-Atmosphere Interactions and Precipitation over the Tropical Ocean Using Observations from AMIE/DYNAMO, Journal of Climate, 29, 8191-8210, 10.1175/jcli-d-16-0040.1, 2016.

Qiu, Y., Liao, H., Zhang, R., and Hu, J.: Simulated impacts of direct radiative effects of scattering and absorbing aerosols on surface layer aerosol concentrations in China during a heavily polluted event in February 2014, Journal of Geophysical Research: Atmospheres, 122, 5955-5975, 10.1002/2016jd026309, 2017.

Randerson, J. T., Van der Werf, G. R., Giglio, L., Collatz, G. J., & Kasibhatla, P. S. (2005). Global Fire Emissions Database, Version 2 (GFEDv2.1), Retrieved from http://daac.ornl.gov/ (last access: 11 November 2013), from Oak Ridge National Laboratory Distributed Active Archive Center, Oak Ridge, TN. https://doi.org/10.3334/ORNLDAAC/849.

Ramanathan, V., Crutzen, P. J., Kiehl, J. T., and Rosenfeld, D.: Aerosols, climate, and the hydrological cycle, Science, 294, 2119-2124, 10.1126/science.1064034, 2001.

Rolph, G. D.: Real-time Environmental Applications and Display System (READY), http://ready.arl.noaa.gov, NOAA Air Resources Laboratory, Silver Spring, MD, 2013.

Shao, Y.: Simplification of a dust emission scheme and comparison with data, Journal of Geophysical Research, 109, 10.1029/2003jd004372, 2004.

Shu, L., Xie, M., Gao, D., Wang, T., Fang, D., Liu, Q., Huang, A., and Peng, L.: Regional severe particle pollution and its association with synoptic weather patterns in the Yangtze River Delta region, China, Atmospheric Chemistry and Physics, 17, 12871-12891, 10.5194/acp-17-12871-2017, 2017.

Skamarock, W. C., Klemp, J. B., Dudhia, J., Gill, D. O., Barker, D. M., Wang, W., and Powers, J. G.: A description of the advanced research WRF version 2, NCAR Tech. Note, NCAR/TN-468+STR, Natl. Cent. Atmos. Res., Boulder, Colo, available at: http://wrf-model.org/wrfadmin/publications.php, 2008.

Steiner, A. L., Mermelstein, D., Cheng, S. J., Twine, T. E., and Oliphant, A.: Observed Impact of Atmospheric Aerosols on the Surface Energy Budget, Earth Interactions, 17, 1-22, 10.1175/2013ei000523.1, 2013.

Su, T., Li, Z., and Kahn, R.: Relationships between the planetary boundary layer height and surface pollutants derived from lidar observations over China: regional pattern and influencing factors, Atmos. Chem. Phys., 18, 15921-15935, 10.5194/acp-18-15921-2018, 2018.

Sun, Y., Jiang, Q., Wang, Z., Fu, P., Li, J., Yang, T., and Yin, Y.: Investigation of the Sources and Evolution Processes of Severe Haze Pollution in Beijing in January 2013, J. Geophys. Res., 119, 4380-4398, 2014.

Sun, Y., Chen, C., Zhang, Y., Xu, W., Zhou, L., Cheng, X., Zheng, H., Ji, D., Li, J., Tang, X., Fu, P., and Wang, Z.: Rapid formation and evolution of an extreme haze episode in Northern China during winter 2015, Scientific reports, 6, 27151, 10.1038/srep27151, 2016.

Sun, J., Huang, L., Liao, H., Li, J., and Hu, J.: Impacts of Regional Transport on Particulate Matter Pollution in China: a Review of Methods and Results, Current Pollution Reports, 3, 182-191, 10.1007/s40726-017-0065-5, 2017.

Tang, G., Zhu, X., Xin, J., Hu, B., Song, T., Sun, Y., Zhang, J., Wang, L., Cheng, M., Chao, N., Kong, L., Li, X., and Wang, Y.: Modelling study of boundary-layer ozone over northern China - Part I: Ozone budget in summer, Atmospheric Research, 187, 128-137, 10.1016/j.atmosres.2016.10.017, 2017.

Tao, W., Liu, J., Ban-Weiss, G. A., Hauglustaine, D. A., Zhang, L., Zhang, Q., Cheng, Y., Yu, Y., and Tao, S.: Effects of urban land expansion on the regional meteorology and air quality of eastern China, Atmos. Chem. Phys., 15, 8597-8614, 10.5194/acp-15-8597-2015, 2015.

Twomey, S.: Pollution and the planetary albedo, Atmos. Environ., 8, 1251-1256, 10.1016/0004-6981(74)90004-3, 1974.

Unger, N., Menon, S., Koch, D. M., and Shindell, D. T.: Impacts of aerosol-cloud interactions on past and future changes in tropospheric composition, Atmos. Chem. Phys., 9, 4115-4129, 10.5194/acp-9-4115-2009, 2009.

Wang, Y., Yao, L., Wang, L., Liu, Z., Ji, D., Tang, G., Zhang, J., Sun, Y., Hu, B., and Xin, J.: Mechanism for the formation of the January 2013 heavy haze pollution episode over central and eastern China, Science China Earth Sciences, 57, 14-25, 10.1007/s11430-013-4773-4, 2013a.

Wang, Z., Li, J., Wang, Z., Yang, W., Tang, X., Ge, B., Yan, P., Zhu, L., Chen, X., Chen, H., Wand, W., Li, J., Liu, B., Wang, X., Wand, W., Zhao, Y., Lu, N., and Su, D.: Modeling study of regional severe hazes over mid-eastern China in January

25

2013 and its implications on pollution prevention and control, Science China Earth Sciences, 57, 3-13, 10.1007/s11430-013-4793-0, 2013b.

Wang, Y., Zhang, Q., Jiang, J., Zhou, W., Wang, B., He, K., Duan, F., Zhang, Q., Philip, S., and Xie, Y.: Enhanced sulfate formation during China's severe winter haze episode in January 2013 missing from current models, Journal of Geophysical Research: Atmospheres, 119, 10,425-410,440, 10.1002/2013jd021426, 2014.

Wang, H., Zhu, B., Shen, L., Xu, H., An, J., Pan, C., Li, Y. e., and Liu, D.: Regional Characteristics of Air Pollutants during Heavy Haze Events in the Yangtze River Delta, China, Aerosol and Air Quality Research, 16, 2159-2171, 10.4209/aaqr.2015.09.0551, 2016a.

Wang, L., Zhang, Y., Wang, K., Zheng, B., Zhang, Q., and Wei, W.: Application of Weather Research and Forecasting Model with Chemistry (WRF/Chem) over northern China: Sensitivity study, comparative evaluation, and policy implications, Atmospheric Environment, 124, 337-350, 10.1016/j.atmosenv.2014.12.052, 2016b.

Wang, Y., Bao, S., Wang, S., Hu, Y., Shi, X., Wang, J., Zhao, B., Jiang, J., Zheng, M., Wu, M., Russell, A. G., Wang, Y., and Hao, J.: Local and regional contributions to fine particulate matter in Beijing during heavy haze episodes, The Science of the total environment, 580, 283-296, 10.1016/j.scitotenv.2016.12.127, 2017.

Wesely, M. L.: Parameterization of surface resistances to gaseous dry deposition in regional-scale numerical models. Atmospheric Environment (1967), 23(6), 1293-1304, 10.1016/0004-6981(89)90153-4, 1989.

Werner, M., Kryza, M., Skjøth, C.A., Kinga, W., Anthony, J.D., Hanna, O., and Jan, K.: Aerosol-radiation feedback and PM10 air concentrations over Poland, Pure Appl. Geophys., 99-110, 10.1007/s00024-016-1267-2, 2016.

Wild, O., Zhu, X., and Prather, M. J.: Fast-J: Accurate Simulation of In and Below-Cloud Photolysis in Tropospheric Chemical Models, J. Atmos. Chem., 37, 245-282, 10.1023/A:1006415919030, 2000.

Wu, L., Su, H., Jiang, J. H., and Read, W. G.: Hydration or dehydration: competing effects of upper tropospheric cloud radiation on the TTL water vapor, Atmospheric Chemistry and Physics, 12, 7727-7735, 10.5194/acp-12-7727-2012, 2012.

Xing, J., Wang, J., Mathur, R., Wang, S., Sarwar, G., Pleim, J., Hogrefe, C., Zhang, Y., Jiang, J., Wong, D. C., and Hao, J.: Impacts of aerosol direct effects on tropospheric ozone through changes in atmospheric dynamics and photolysis rates, Atmos Chem Phys, 17, 9869-9883, 10.5194/acp-17-9869-2017, 2017.

Yahya, K., Wang, K., Gudoshava, M., Glotfelty, T., and Zhang, Y.: Application of WRF/Chem over North America under the AQMEII Phase 2: Part I. Comprehensive evaluation of 2006 simulation, Atmospheric Environment, 115, 733-755, 10.1016/j.atmosenv.2014.08.063, 2015.

Yang, J., Duan, K., Kang, S., Shi, P., and Ji, Z.: Potential feedback between aerosols and meteorological conditions in a heavy pollution event over the Tibetan Plateau and Indo-Gangetic Plain, Climate Dynamics, 48, 2901-2917, 10.1007/s00382-016-3240-2, 2016a.

Yang, Y., Liao, H., and Lou, S.: Increase in winter haze over eastern China in recent decades: Roles of variations in meteorological parameters and anthropogenic emissions, Journal of Geophysical Research: Atmospheres, 121, 13,050-013,065, 10.1002/2016jd025136, 2016b.

Yang, Y., Russell, L.M., Lou, S., Liao, H., Guo, J., Liu, Y., Singh, B., and Ghan, S.J.: Dust-wind interactions can intensify aerosol pollution over eastern China, Nat. Commun., 8, 15333, 10.1038/ncomms15333, 2017.

Zaveri, R. A., and Peters, L. K.: A new lumped structure photochemical mechanism for large-scale applications, Journal of Geophysical Research: Atmospheres, 104, 30387-30415, 10.1029/1999jd900876, 1999.

Zaveri, R. A., Easter, R. C., Fast, J. D., and Peters, L. K.: Model for Simulating Aerosol Interactions and Chemistry (MOSAIC), Journal of Geophysical Research, 113, 10.1029/2007jd008782, 2008.

Zhang, Y., Dubey, M. K., Olsen, S. C., Zheng, J., and Zhang, R.: Comparisons of WRF/Chem simulations in Mexico City with ground-based RAMA measurements during the 2006-MILAGRO, Atmos. Chem. Phys., 9, 3777-3798, 10.5194/acp-9-3777-2009, 2009.

Zhang, Y., Chen, Y., Sarwar, G., and Schere, K.: Impact of gas-phase mechanisms on Weather Research Forecasting Model with Chemistry (WRF/Chem) predictions: Mechanism implementation and comparative evaluation, Journal of Geophysical Research: Atmospheres, 117, n/a-n/a, 10.1029/2011jd015775, 2012.

Zhang, B., Wang, Y., and Hao, J.: Simulating aerosol–radiation–cloud feedbacks on meteorology and air quality over eastern China under severe haze conditions in winter, Atmos. Chem. Phys., 15, 2387-2404, acp-15-2387-2015, 2015a.

Zhang, L., Liu, L., Zhao, Y., Gong, S., Zhang, X., Henze, D. K., Capps, S. L., Fu, T.-M., Zhang, Q., and Wang, Y.: Source

attribution of particulate matter pollution over North China with the adjoint method, Environmental Research Letters, 10, 084011, 10.1088/1748-9326/10/8/084011, 2015b.

Zhang, R., Sun, X., Shi, A., Huang, Y., Yan, J., Nie, T., Yan, X., and Li, X.: Secondary inorganic aerosols formation during haze episodes at an urban site in Beijing, China, Atmospheric Environment, 177, 275-282, 10.1016/j.atmosenv.2017.12.031, 2018a.

Zhang, Z., Xu, X., Qiao, L., Gong, D., Kim, S. J., Wang, Y., and Mao, R.: Numerical simulations of the effects of regional topography on haze pollution in Beijing, Scientific reports, 8, 5504, 10.1038/s41598-018-23880-8, 2018b.

Zhang, L., Guo, X., Zhao, T., Gong, S., Xu, X., Li, Y., Luo, L., Gui, K., Wang, H., Zheng, Y., and Yin, X.: A modelling study of the terrain effects on haze pollution in the Sichuan Basin, Atmospheric Environment, 196, 77-85, 10.1016/j.atmosenv.2018.10.007, 2019.

Zhao, C., Liu, X., Leung, L. R., Johnson, B., McFarlane, S. A., Gustafson, W. I., Fast, J. D., and Easter, R.: The spatial distribution of mineral dust and its shortwave radiative forcing over North Africa: modeling sensitivities to dust emissions and aerosol size treatments, Atmospheric Chemistry and Physics, 10, 8821-8838, 10.5194/acp-10-8821-2010, 2010.

Zhao, C., Liu, X., Ruby Leung, L., and Hagos, S.: Radiative impact of mineral dust on monsoon precipitation variability over West Africa, Atmospheric Chemistry and Physics, 11, 1879-1893, 10.5194/acp-11-1879-2011, 2011.

Zhao, C., Ruby Leung, L., Easter, R., Hand, J., and Avise, J.: Characterization of speciated aerosol direct radiative forcing over California, Journal of Geophysical Research: Atmospheres, 118, 2372-2388, 10.1029/2012jd018364, 2013.

Zhao, B., Liou, K. N., Gu, Y., Li, Q., Jiang, J. H., Su, H., He, C., Tseng, H. R., Wang, S., Liu, R., Qi, L., Lee, W. L., and Hao, J.: Enhanced PM2.5 pollution in China due to aerosol-cloud interactions, Scientific reports, 7, 4453, 10.1038/s41598-017-04096-8, 2017.

Zhao, S., Yu, Y., Yin, D., Qin, D., He, J., and Dong, L.: Spatial patterns and temporal variations of six criteria air pollutants during 2015 to 2017 in the city clusters of Sichuan Basin, China, The Science of the total environment, 624, 540-557, 10.1016/j.scitotenv.2017.12.172, 2018.

Zheng, G. J., Duan, F. K., Su, H., Ma, Y. L., Cheng, Y., Zheng, B., Zhang, Q., Huang, T., Kimoto, T., Chang, D., Pöschl, U., Cheng, Y. F., and He, K. B.: Exploring the severe winter haze in Beijing: the impact of synoptic weather, regional transport and heterogeneous reactions, Atmospheric Chemistry and Physics, 15, 2969-2983, 10.5194/acp-15-2969-2015, 2015.

Zheng, B., Tong, D., Li, M., Liu, F., Hong, C., Geng, G., Li, H., Li, X., Peng, L., Qi, J., Yan, L., Zhang, Y., Zhao, H., Zheng, Y., He, K., and Zhang, Q.: Trends in China's anthropogenic emissions since 2010 as the consequence of clean air actions, Atmos. Chem. Phys., 18, 14095-14111, acp-18-14095-2018, 2018.

Zhou, M., Zhang, L., Chen, D., Gu, Y., Fu, T.-M., Gao, M., Zhao, Y., Lu, X., and Zhao, B.: The impact of aerosol-radiation interactions on the effectiveness of emission control measures, Environmental Research Letters, 10.1088/1748-9326/aaf27d, 2018.

Zhu, B., Kang, H. Q., Zhu, T., Su, J. F., Hou, X. W., and Gao, J. H.: Impact of Shanghai urban land surface forcing on downstream city ozone chemistry, J. Geophys. Res.-Atmos., 120, 4340-4351, 10.1002/2014JD022859, 2015.

Zhu, J., Chen, L., Liao, H., and Dang, R.: Correlations between PM2.5 and Ozone over China and Associated Underlying Reasons, Atmosphere, 1-15, 352 (10), 10.3390/atmos10070352, 2019.

Table 1. Parameterizations used in the WRF-Chem model

Options	WRF-Chem
Microphysics option	Purdue Lin scheme
Longwave radiation option	RRTMG scheme
Shortwave radiation option	RRTMG scheme
Surface layer option	Revised MM5 Monin-Obukhov scheme
Land surface option	Unified Noah land-surface model
Urban canopy model	Single-layer UCM scheme
Boundary layer option	YSU scheme
Cumulus option	Grell 3D ensemble scheme
Photolysis scheme	Fast-J
Dust scheme	Shao_2004
Chemistry option	CBMZ
Aerosol option	MOSAIC
Analysis nudging	On

Table 2. Experimental design

Case Description	Anthropogenic Emission	Aerosol Direct Effect	Aerosol Indirect Effect
CTL	Y	Y	Y
NoAnth	Without emission in the whole domain	Y	Y
NoBTH_Anth	Without emission in BTH	Y	Y
OnlyBTH_Anth	Only emission in BTH	Y	Y
NoARE	Y	N	N

Table 3. Statistical metrics between observations and simulations

Variables	nstd	$\overline{\text{OBS}}$[1]	$\overline{\text{SIM}}$[2]	NMB[3]	MFB[4]	MFE[5]	IOA[6]	R[7]
T_2 (k)[a]	12	270.7	271.6	1	1	1	0.94	0.90
RH_2 (%)[a]	12	63.8	56.1	-12	-12	22	0.82	0.73
WS_{10} (m s^{-1})[a]	12	2.5	3.2	28	32	58	0.79	0.70
WD_{10} (°)[a]	12	190.8	192.2	1	-2	55	0.65	0.43
$\text{PM}_{2.5}$ (µg m^{-3})	59	173.6	168.2	-3	13	47	0.86	0.76

[a]T_2: temperature at 2 m (k); RH_2: relative humidity at 2 m (%); WS_{10}: wind speed at 10 m (m s^{-1}); WD_{10}: wind direction at 10 m (°).

[1,2]$\overline{\text{OBS}}$ and $\overline{\text{SIM}}$ represent the average observations and simulations, respectively. $\overline{\text{OBS}} = \frac{1}{\text{nstd}} \times \sum_{i=1}^{\text{nstd}} \text{OBS}_i$, $\overline{\text{SIM}} = \frac{1}{\text{nstd}} \times \sum_{i=1}^{\text{nstd}} \text{SIM}_i$.

[3]NMB is the normalized mean bias, $\text{NMB} = \frac{1}{\text{nstd}} \times \sum_{i=1}^{\text{nstd}} \frac{\text{SIM}_i - \text{OBS}_i}{\text{OBS}_i} \times 100\%$.

5

[4]MFB is the mean fractional bias, $\text{MFB} = \frac{2}{\text{nstd}} \times \sum_{i=1}^{\text{nstd}} \frac{\text{SIM}_i - \text{OBS}_i}{\text{SIM}_i + \text{OBS}_i} \times 100\%$.

[5]MFE is the mean fractional error, $\text{MFE} = \frac{2}{\text{nstd}} \times \sum_{i=1}^{\text{nstd}} \frac{|\text{SIM}_i - \text{OBS}_i|}{\text{SIM}_i + \text{OBS}_i} \times 100\%$.

[6]IOA is the index of agreement, $\text{IOA} = 1 - \frac{\sum_{i=1}^{\text{nstd}} (\text{SIM}_i - \text{OBS}_i)^2}{\sum_{i=1}^{\text{nstd}} (|\text{OBS}_i - \overline{\text{OBS}}| + |\text{SIM}_i - \overline{\text{SIM}}|)^2}$.

[7]R is the correlation coefficient, $R = \frac{\sum_{i}^{\text{nstd}} |(\text{OBS}_i - \overline{\text{OBS}}) \times (\text{SIM}_i - \overline{\text{SIM}})|}{\sqrt{\sum_{i}^{\text{nstd}} (\text{OBS}_i - \overline{\text{OBS}})^2 + \sum_{i}^{\text{nstd}} (\text{SIM}_i - \overline{\text{SIM}})^2}}$.

Where OBS_i and SIM_i mean observations and model predictions, respectively. i refers to a given station, and nstd is the total number
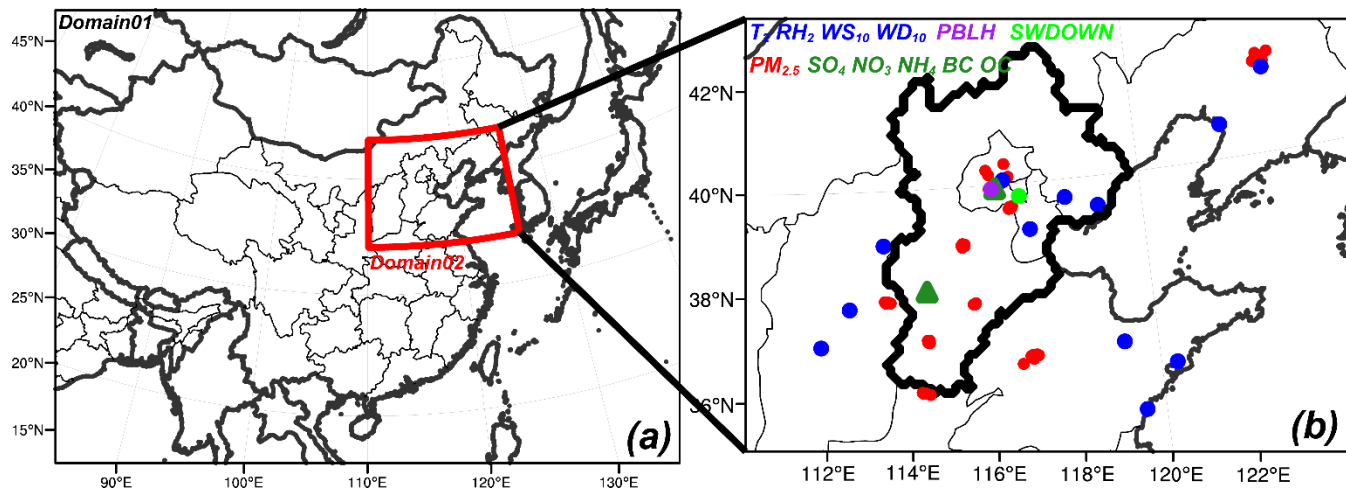
10 of stations.

Figure 1. (a) Map of the two nested model domains. (b) Locations of the observations used for model evaluation.
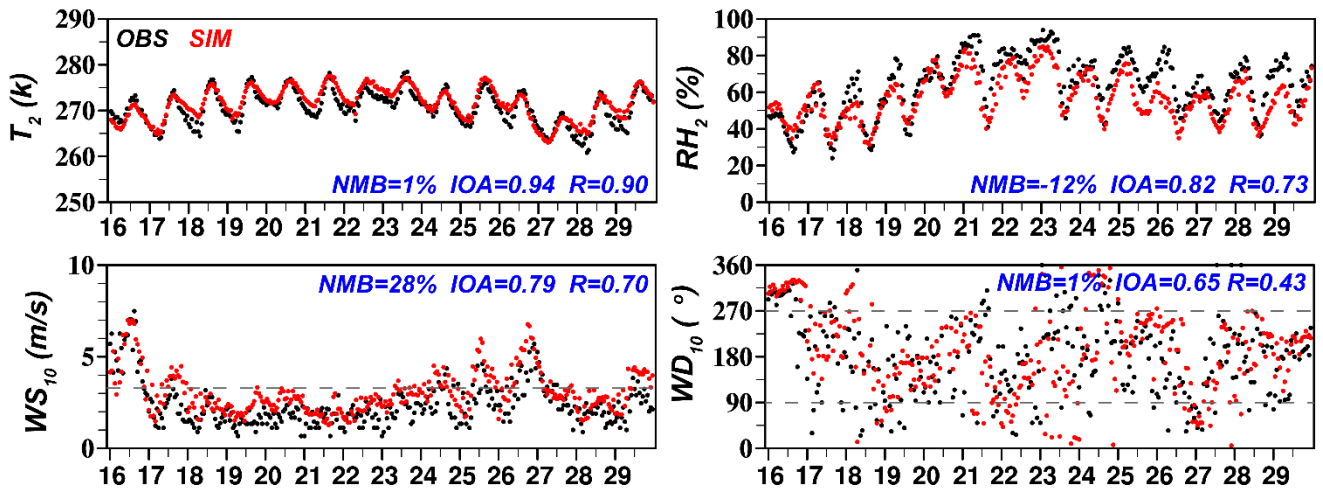
5

Figure 2. Time series of observed (shown in black dots) and simulated (shown in red dots) hourly 2 m temperature (T_2, k), 2 m relative humidity (RH_2, %), 10 m wind speed (WS_{10}, m s^{-1}), and 10 m wind direction (WD_{10}, ％) averaged over the 12 stations during 16-29 December 2015.
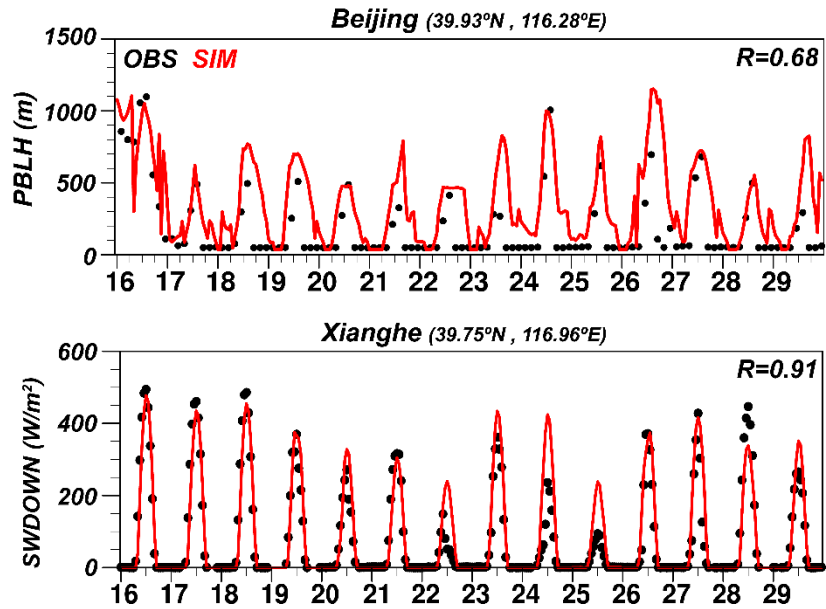
Figure 3. Time series of observed (shown in black dots) and simulated (shown in red lines) hourly planetary boundary layer height (PBLH, m) at the site of (39.93 °N, 116.28 °E) in Beijing, and shortwave downward radiation flux (SWDOWN, W m⁻²) at the Xianghe Station (39.75 °N, 116.96 °E) from 16 to 29 December 2015. Notably, PBLH provided by Global Data Assimilation System (GDAS) are in 3-hour intervals. All the time is converted to China Standard Time (Beijing Time).
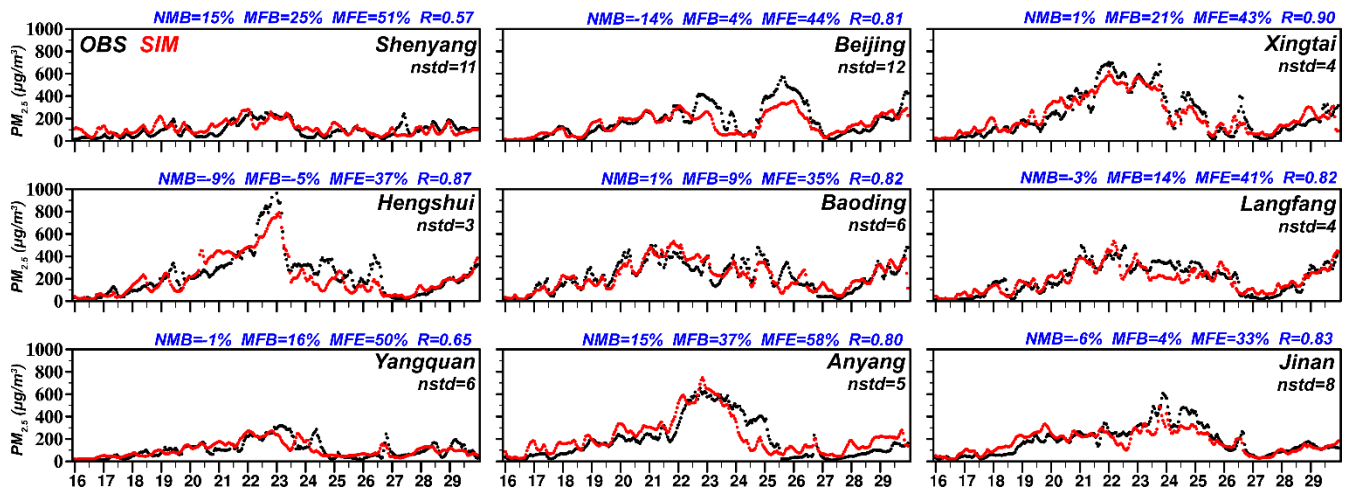
Figure 4. Time series of observed (shown in black dots) and simulated (shown in red dots) hourly PM$_{2.5}$ concentrations (μg m^{-3}) in the nine cities (Shengyang, Beijing, Xingtai, Hengshui, Baoding, Langfang, Yangquan, Anyang, and Jinan) from 16 to 29 December 2015. The nstd in each panel represents the number of observation sites in each city. Beijing Time is used for these hourly time series.
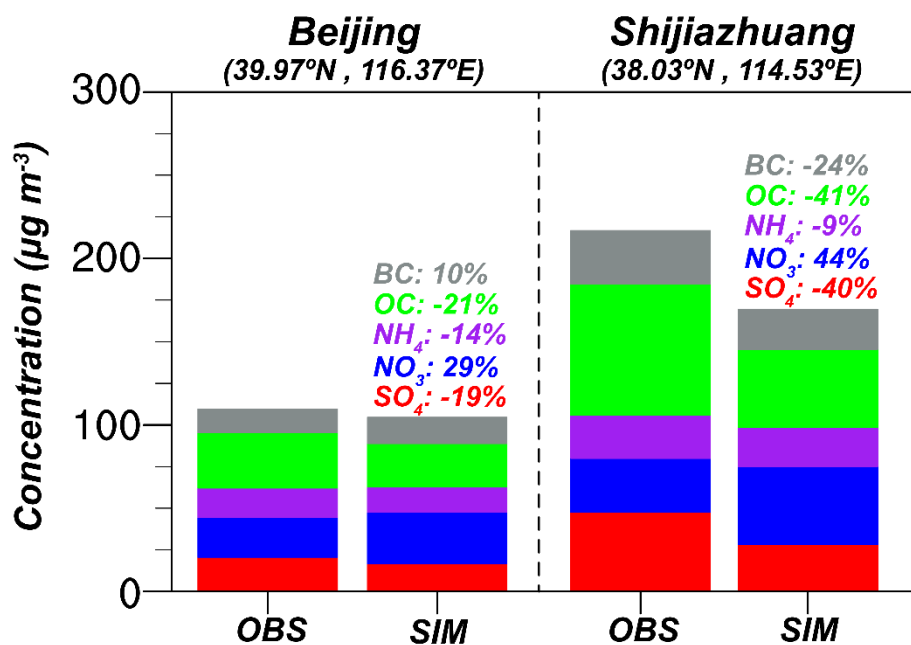
Figure 5. Comparison of observed and simulated surface-layer mass concentrations (μg m^{-3}) of SO_4^{2-} (red), NO_3^- (blue), NH_4^+ (purple), OC (green), and BC (gray) in the sites of (a) (39.97 °N, 116.37 °E) in Beijing, and (b) (38.03 °N, 114.53 °E) in Shijiazhuang averaged over 16-29 December 2015. Also listed in colored numbers are normalized mean biases (NMBs) for each species.
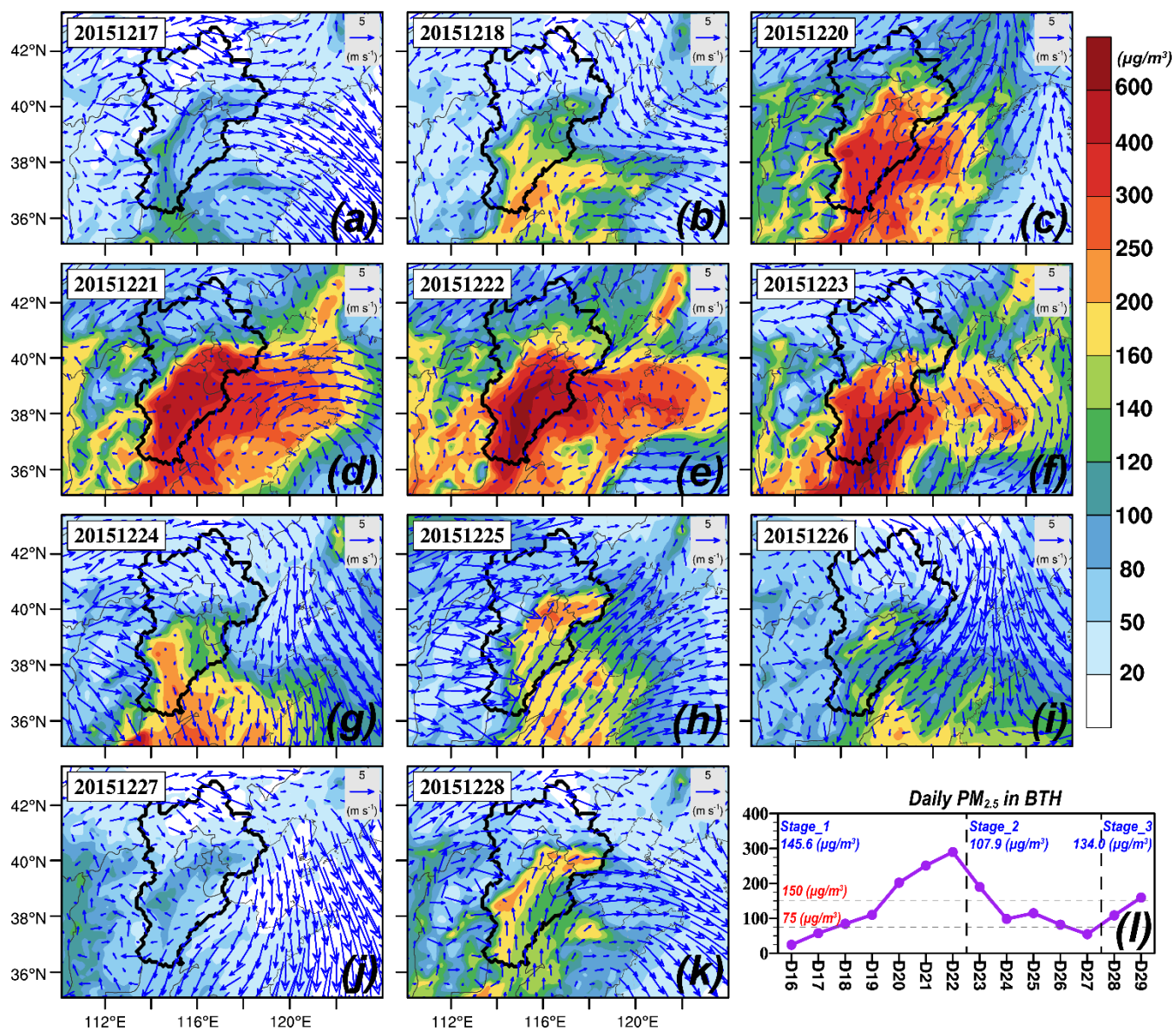
Figure 6. (a-k) Spatial distributions of simulated daily PM$_{2.5}$ concentrations (shaded, μg m^{-3}) and wind vectors (arrows, m s^{-1}). Time series of simulated daily PM$_{2.5}$ concentrations averaged over the Beijing-Tianjin-Hebei region are also shown in (l).

5
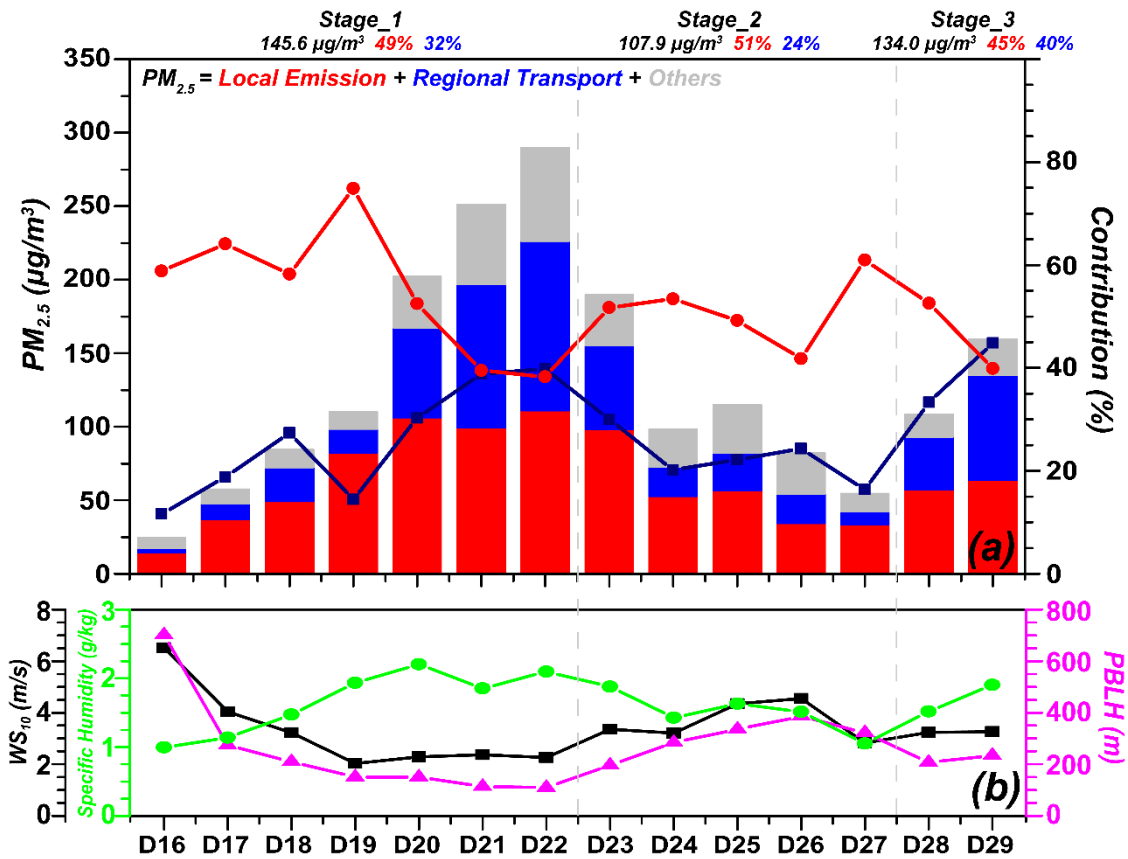
Figure 7. (a) Contributions of local emission (shown in red) and regional transport (shown in blue) to the near-surface $PM_{2.5}$ concentrations averaged over the Beijing-Tianjin-Hebei region from 16 to 29 December 2015. The absolute contributions ($\mu g\ m^{-3}$) are shown in bars, and the percentage contributions (%) are shown in lines. The $PM_{2.5}$ concentration and the percentage contributions averaged over each stage are listed at the top of (a). Simulated daily 10 m wind speed (WS_{10}, m s^{-1}, shown in black dot line), specific humidity (g kg^{-1}, shown in green dot line), and PBLH (m, shown in purple dot line) averaged over Beijing-Tianjin-Hebei are also shown in (b).
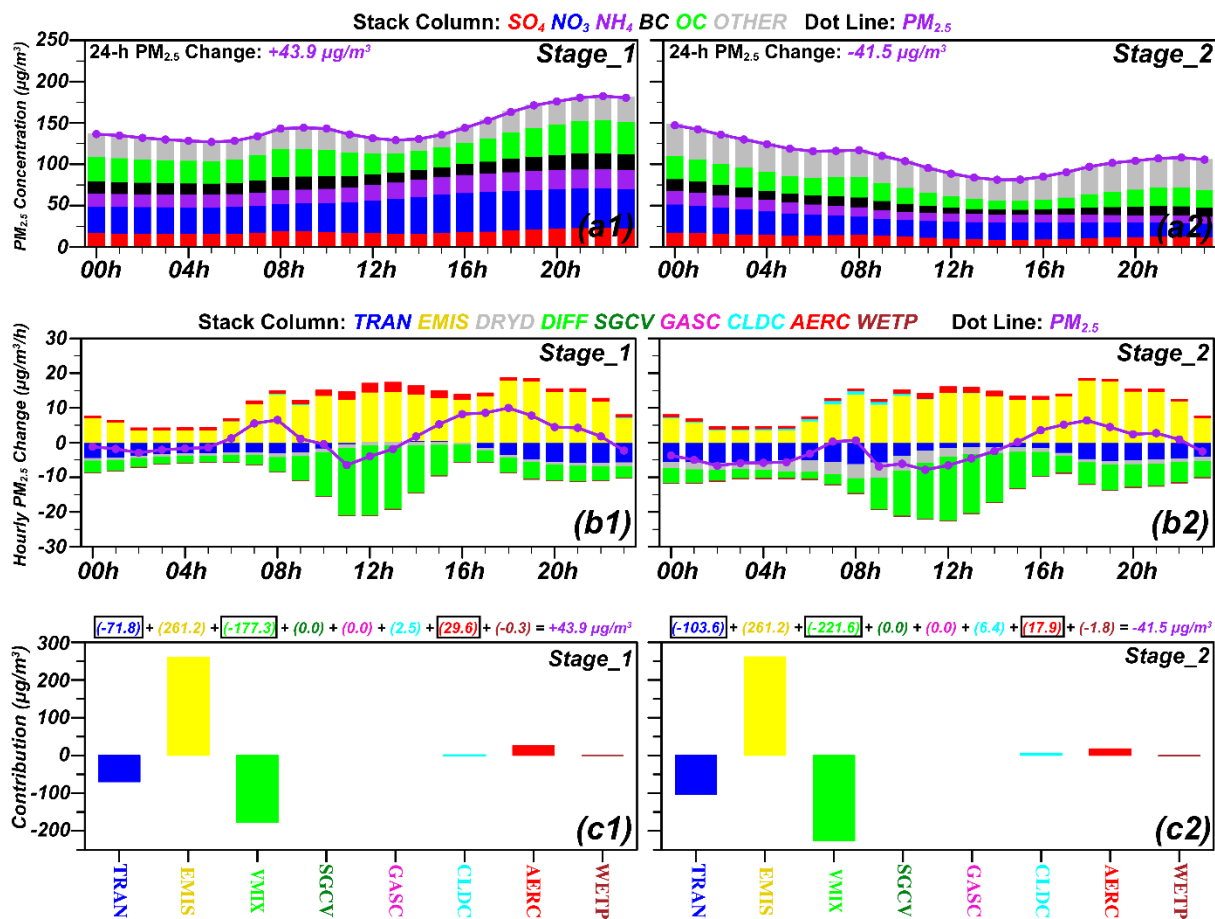
Figure 8. (a1-a2) Diurnal variations of PM₂.₅ concentrations averaged over Beijing-Tianjin-Hebei during Stage_1 and Stage_2 (shown by purple dot lines). The colored bars represent different components. Also shown at the top left corner of each panel is the 24-h change in PM₂.₅ concentration (23:00LST minus 00:00LST). **(b1-b2)** The hourly PM₂.₅ changes induced by each physical/chemical process by using the IPR analysis method (shown by colored bars). The purple dot lines represent hourly PM₂.₅ changes induced by all processes, also indicating the differences between current and previous-hour PM₂.₅ concentrations. **(c1-c2)** Contributions of each physical/chemical process to 24-h PM₂.₅ changes.
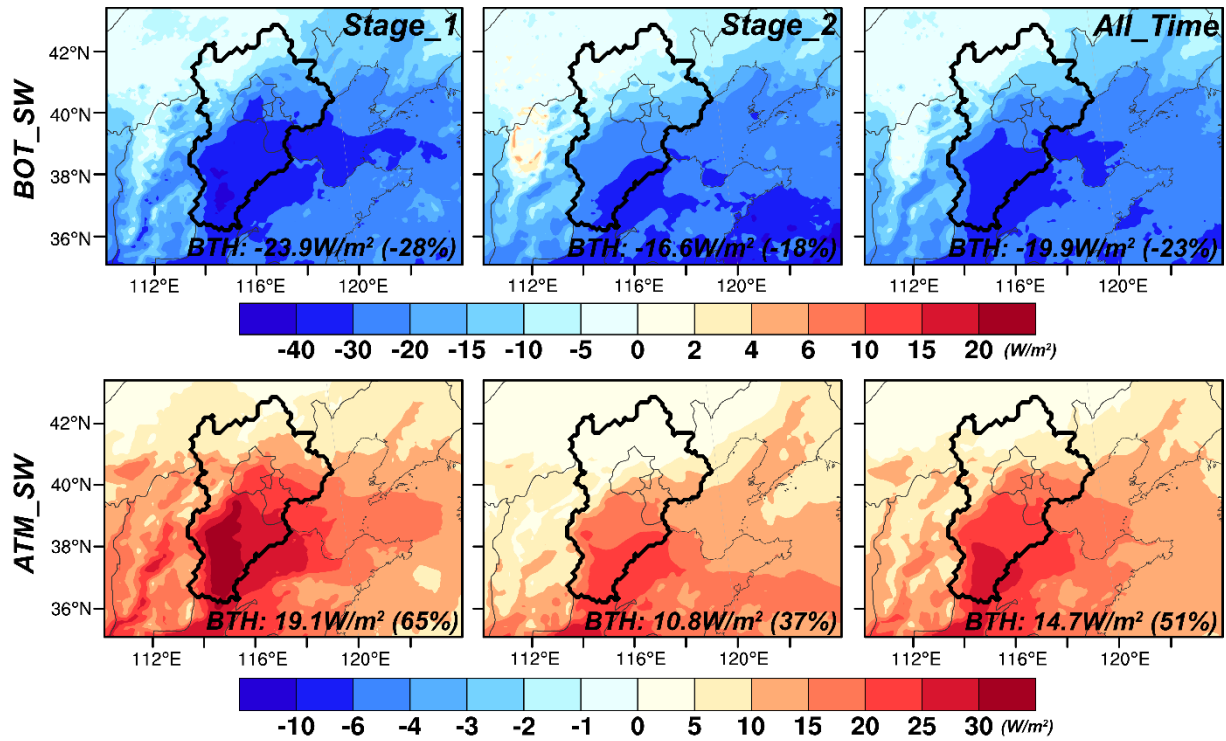
Figure 9. The differences in simulated all-sky radiative forcing (W m^{-2}) between CTL and NoARE cases (CTL minus NoARE) averaged over Stage_1, Stage_2, and the whole simulation period. "BOT_SW" and "ATM_SW" denote the downward shortwave radiative flux at the surface and in the atmosphere, respectively. The calculated differences in the simulated radiative forcing averaged over Beijing-Tianjin-Hebei for each stage are also shown at the bottom of each panel.
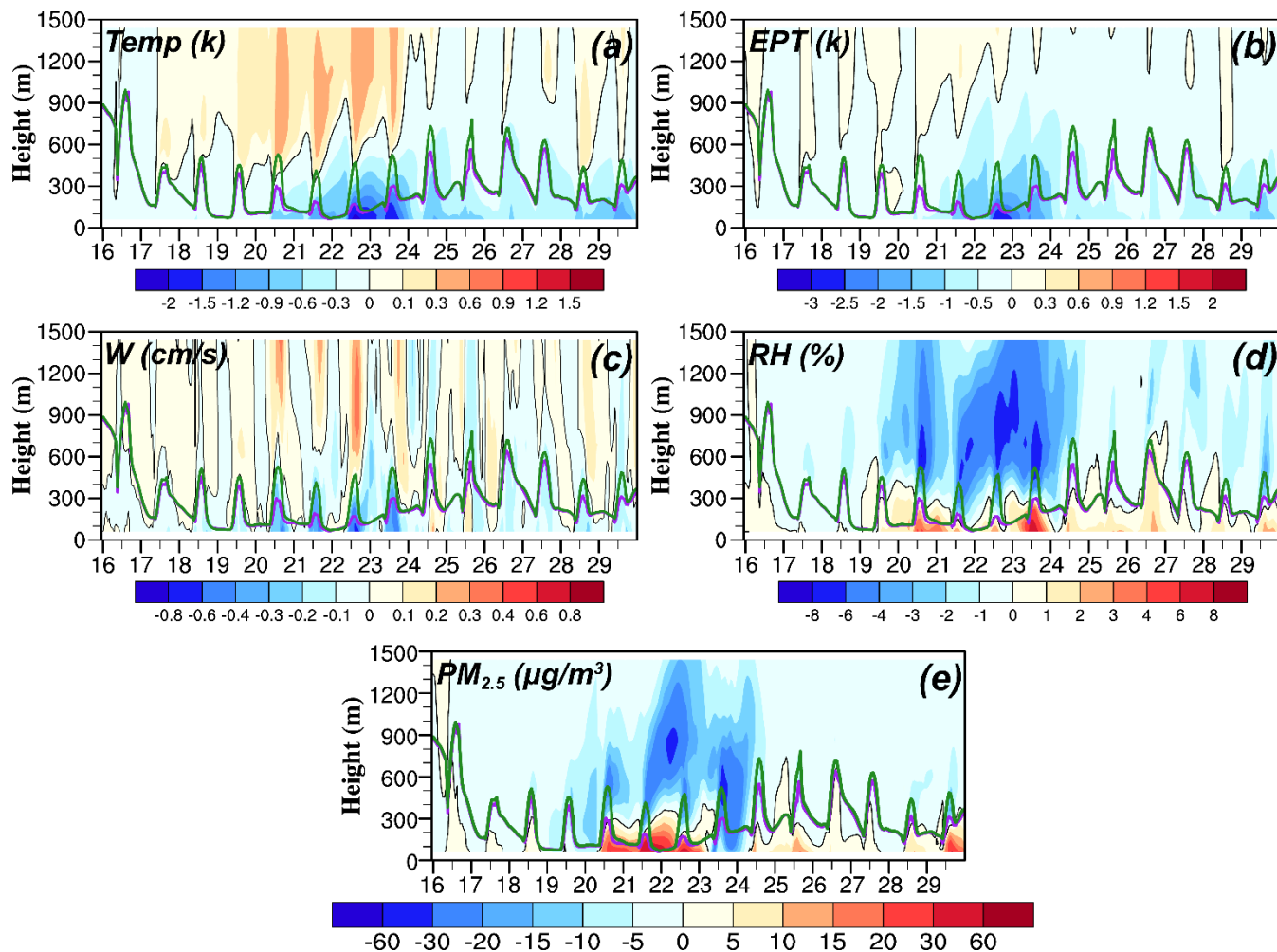
Figure 10. Time series of differences in (a) temperature (k), (b) equivalent potential temperature (k), (c) vertical wind speed (cm s^{-1}), (d) relative humidity (%), and (e) PM$_{2.5}$ concentration (μg m^{-3}) between CTL and NoARE cases (CTL minus NoARE) averaged over the Beijing-Tianjin-Hebei region. The purple and green lines denote the simulated PBLH in CTL and NoARE cases, respectively. The black line represents the zero contour line.
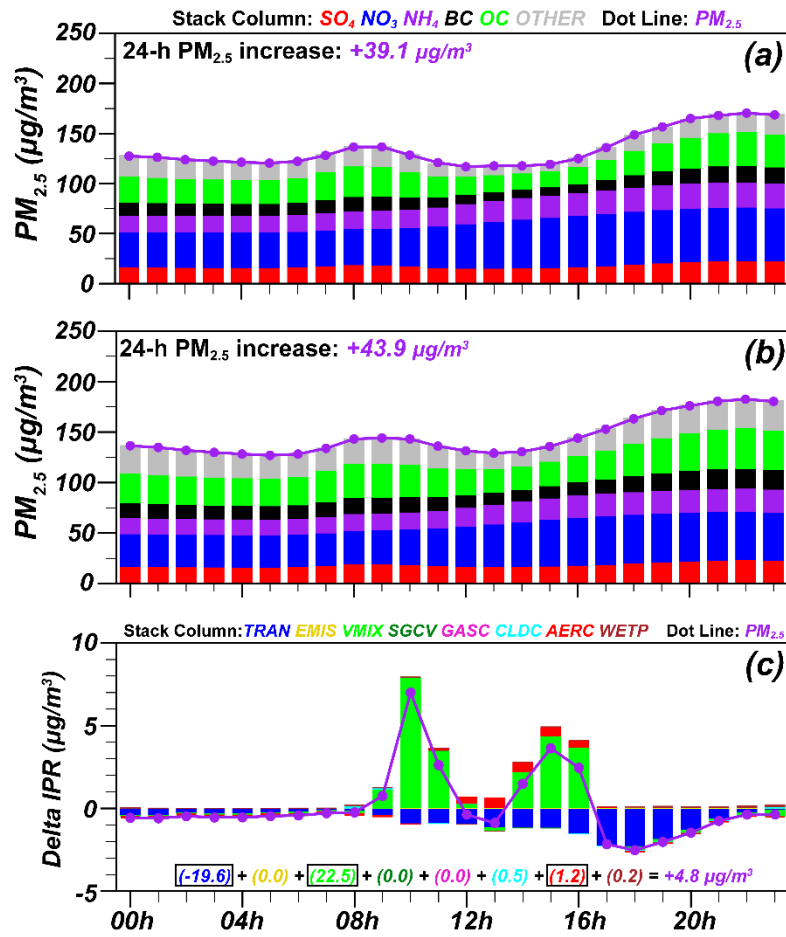
Figure 11. Diurnal variations of the near-surface PM$_{2.5}$ concentrations in (a) NoARE and (b) CTL simulations averaged over the Beijing-Tianjin-Hebei region during Stage_1 (shown by purple dot lines). The colored bars represent different components. Also shown at the top left corner of each panel is the 24-h increase in PM$_{2.5}$ concentration (23:00LST minus 00:00LST). (c) Differences in hourly IPRs caused by aerosol radiative forcing (CTL minus NoARE). The numbers listed in (c) represent the contributions of each process to the change in 24-h PM$_{2.5}$ increase caused by aerosol radiative forcing.
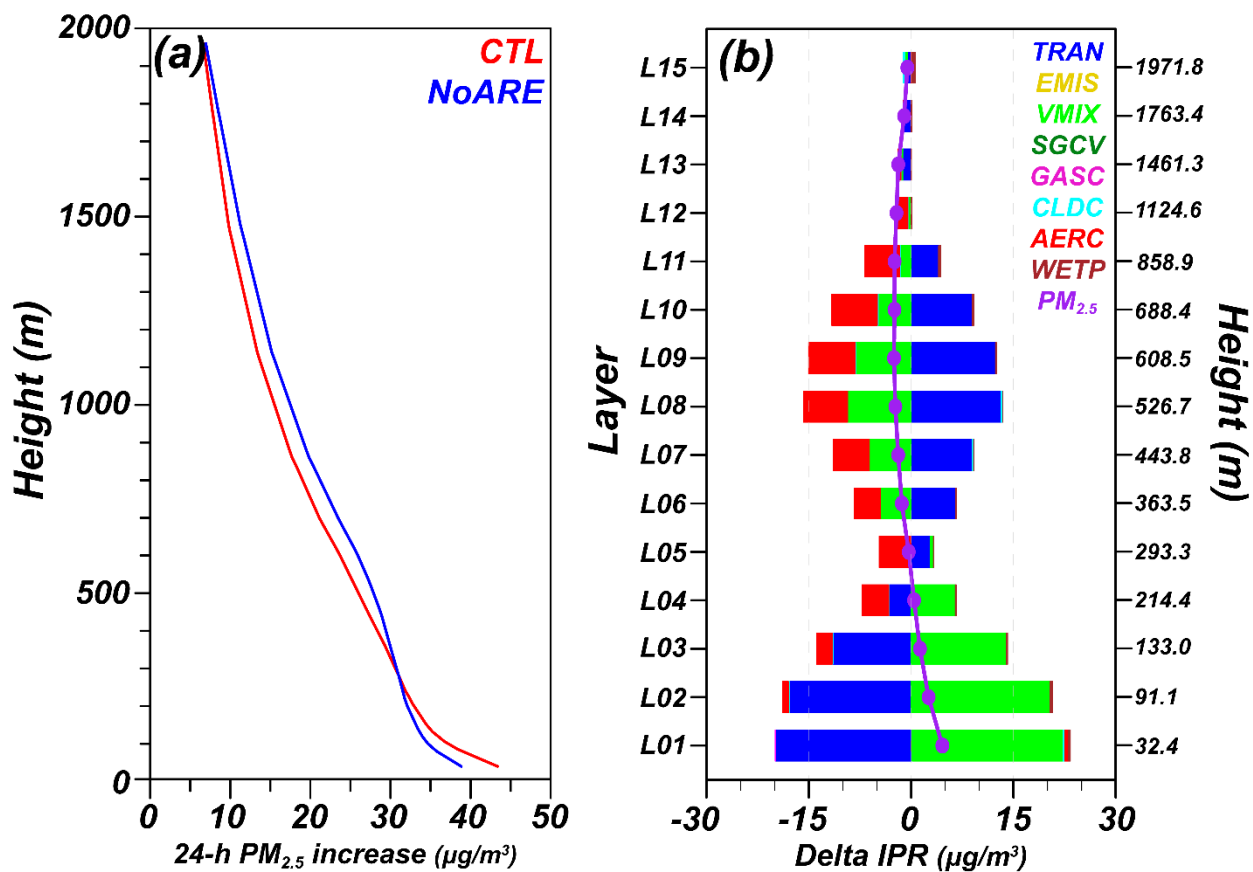
Figure 12. (a) Vertical profiles of the 24-h increases in PM$_{2.5}$ concentrations (23:00LST minus 00:00LST) averaged over Beijing-Tianjin-Hebei during Stage_1 in CTL and NoARE cases. (b) Vertical profiles of the differences in the 24-h PM$_{2.5}$ increases caused by aerosol radiative effect (CTL minus NoARE, as show in purple dot line), and the contributions of each physical/chemical process (as shown in colored bars).